Received: 25 November 2019 | Revised: 7 May 2020 | Accepted: 14 May 2020

DOI: 10.1002/arp.1782

RESEARCH ARTICLE

WILEY

What over 100 drillings tell us: a new method for determining the Koenigsberger ratio of soils from magnetic mapping and susceptibility logging

Natalie Pickartz[1,2] | Wolfgang Rabbel[1,2] | Knut Rassmann[3] | Nils Müller-Scheeßel[4] | Martin Furholt[5] | Johannes Müller[2,4] | Ivan Cheben[6] | Dennis Wilken[1,2] | Tina Wunderlich[1,2] | Stefan Dreibrodt[2,7]

[1]Institute of Geosciences, Kiel University, Kiel, Germany

[2]Collaborative Research Center 1266, Kiel University, Kiel, Germany

[3]Romano-Germanic Commission, German Archaeological Institute, Frankfurt am Main, Germany

[4]Institute of Prehistoric and Protohistoric Archaeology, Kiel University, Kiel, Germany

[5]Department of Archaeology, Conservation and History, University of Oslo, Oslo, Norway

[6]Archaeological Institute, Slovak Academy of Sciences, Nitra, Slovakia

[7]Institute for Ecosystem Research, Kiel University, Kiel, Germany

Correspondence
Institute of Geosciences, Kiel University. Kiel, 24118, Germany.
Email: natalie.pickartz@ifg.uni-kiel.de

Funding information
Deutsche Forschungsgemeinschaft, Grant/Award Number: Project Number 2901391021; Vedecká Grantová Agentúra MŠVVaŠ SR a SAV, Grant/Award Number: VEGA-Project 2/0107/17

Abstract

We investigate the relative fractions of remanent and induced magnetization of the fillings of neolithic long pits in order to develop remanent magnetization as an additional parameter for the archaeological interpretation of magnetic maps. We determine the Koenigsberger ratio – the ratio between induced and remanent magnetization intensities – for key targets by combining magnetic mapping with downhole measurements of susceptibility, numerical modelling, and inversion computations. The susceptibility data were acquired in drill holes along profiles crossing the targets identified by magnetic mapping. The targets of this exemplary study are house-accompanying pits at the Linearbandkeramik site Vráble 'Farské'. For this purpose, we conducted auger drillings with a point distance of 25 cm and measured the susceptibility with a downhole susceptometer. The resulting two-dimensional susceptibility distributions were used to calculate synthetic magnetic anomalies corresponding to the case of solely induced magnetization. The comparison to the observed magnetic data showed a considerable discrepancy that can only be explained with remanent magnetization. To determine the Koenigsberger ratio we developed a new interpretation approach, using parts of the measured susceptibility distribution as a basis function. The free parameters of this numerical problem are determined by non-linear inversion. We applied the novel approach to six exemplary profiles and found Koenigsberger ratios between 1.6 and 10.5 with the majority of the values being smaller than 4. These values apply to soil volumes with susceptibility values larger than 27–160 $\times$ 10^{-5} SI. Laboratory measurements on soil samples were used to examine the possible causes of the observed magnetization. The analyses suggest that the increase in susceptibility and remanent magnetization in the pits is caused by an increase of the population of magnetotactic bacteria and deposition of magnetized material, followed by the alignment of the ferrimagnetic iron compounds in the waterlogged environment of the pits and accumulation of viscous remanent magnetization.

KEYWORDS
Koenigsberger ratio, magnetic susceptibility, inversion, forward modelling, Linearbandkeramik (LBK) longpits, magnetotatic bacteria

1 | INTRODUCTION

The title of this article suggests two questions, which guide the present study: Why should we want to determine the Koenigsberger ratio in an archaeological context? And how can we determine it from field measurements?

The Koenigsberger ratio Q is the ratio between remanent and induced magnetization (Koenigsberger, 1930, 1934, 1936). It characterizes the relative importance of the remanent magnetization to be considered in a quantitative interpretation of magnetic anomalies and can be regarded as a parameter of archaeological relevance (Fassbinder, 2015). However, the contribution to the observed magnetic anomalies resulting from remanent magnetization is often neglected infield studies if effects of remanence are not obvious in the magnetic map. In this context, exceptionally strong amplitude anomalies and significant azimuthal deviations of the magnetic field vector from the ambient field may be regarded as obvious indications, such as resulting from thermoremanent magnetization of kilns, ovens and displaced bricks.

Case studies often approach a quantitative interpretation of magnetic anomalies using the assumptions of a simplified source geometry and induced-only magnetization. To explain the observed data, the susceptibility contrast between the source and the surrounding subsurface matrix is then determined for this geometry by linear inversion (Miller et al., 2019; Schneider et al., 2014; Wilken, Wunderlich, Majchczack, Andersen, & Rabbel, 2015).

In archaeomagnetic and archaeological case studies, the Koenigsberger ratio is usually determined via measurements of the magnetic susceptibility and the natural remanent magnetization (NRM) of samples. These studies have been conducted in the laboratory on samples from archaeological sites that had been exposed to heating (Carrancho et al., 2009; Catanzariti et al., 2008; Ertepinar et al., 2016; Gómez-Paccard et al., 2006; Herries, Kovacheva, & Kostadinova, 2008; Hunt, Moskowitz, & Banerjee, 2013; Jordanova, Kovacheva, & Kostadinova, 2004; Kapper et al., 2014; Kapper, Donadini, Mauvilly, Panovska, & Hirt, 2014; Linford & Canti, 2001; Schnepp et al., 2004; Schnepp & Pucher, 1998). For example, Q varies between values of 0.1 for granite and 100 for mud-bricks (Ertepinar et al., 2016), between 0.1 and 100 for different kind of kilns, baths, hypocausts and furnaces (Gómez-Paccard et al., 2006; Schnepp et al., 2004) or 0.7 and 10 with values up to 250 in the context of combustion levels (Kapper, Anesin, et al., 2014). (Kapper, Donadini, et al., 2014) found values between 0.1 and 10 for burned cave sediments.

Jrad et al. (2014) presented a comparison of measurements of the magnetic properties of palaeohearths and an experimental hearth. For the experimental hearth, they derived values of Q between 0.3 and 3.5 by susceptibility and NRM measurements, where the highest values were reached in the first centimetres below the surface. They could reproduce the observed magnetic anomaly of two paleaohearts with a subsurface model consisting of four layers (ash, base, soil, limestone pebbles). The derived values for Q turned out to be in the same range as the measured ones.

Benech, Tabbagh, and Desvignes (2002) presented a filtering process of magnetic and electromagnetic data to separate the induced and remanent portions of magnetization, which is applicable if the magnetic structure is fully located within the depth of investigation of the electromagnetic probe. From the filter output a bulk Koenigsberger ratio can be deduced.

Apart from thermoremanent magnetization, detrital or depositional remanent magnetization (DRM) can occur in the context of archaeological pits and ditches or more general in ground depressions. The anomalies are rather weak but detectable (Fassbinder, 2015). DRM develops trough alignment of remanent magnetized particles in the direction of the earth's magnetic field if they are mobile in the pore water (Evans & Heller, 2003; Fassbinder, 2015). At intra-particle scales viscous remanent magnetization (VRM) is acquired over long periods under moderate ambient temperature conditions. VRM accumulates through random thermal fluctuations of the magnetic moments that subsequently align parallel to the present earth's magnetic field and stay in this orientation (Néel, 1955).

In this article, we show the importance of remanent magnetization for the magnetization of soils. This is a case where magnetic maps usually do not show obvious evidence of a contribution of remanent magnetization because the anomalies of soil-filled pits are usually only low or moderate in amplitude and only slightly, if at all, deviated from the present declination. We present a novel approach to determine the Koenigsberger ratio from magnetic prospection data and downhole susceptibility measurements. In this approach neither sampling nor NRM measurements are necessary. Our study targets magnetic anomalies arising from long-pits that accompany houses belonging to the neolithic Linear Pottery culture at the site Vráble 'Farské' (Slovakia). We base our study on susceptibility-depth sections crossing the magnetic anomalies that were gathered with dense downhole measurements. These two-dimensional susceptibility distributions clearly show the cross-section of the pits and are used as empirical subsurface models to calculate related synthetic magnetic anomalies. Hence, based on the in-phase susceptibility, measured at 1.3 kHz, the induced magnetization is calculated. In turn, the induced magnetization yields the base for the calculation of the synthetic magnetic data. A comparison of the synthetic and observed magnetic data shows a discrepancy that can be explained with an additional remanent magnetization. From the susceptibility distribution we derive spatial basis functions for an inversion calculation, by which the Koenigsberger

ratio is determined. Additional laboratory analyses are conducted to determine low and high frequency magnetic susceptibility, iron content, loss-on-ignition (LOI), soil colour, X-ray fluorescence (XRF) and X-ray diffraction (XRD). These enable an understanding of the measured susceptibility distributions as such and of environmental and archaeological factors related to the site formation.

This article is structured as follows: First, general information on the archaeological example site and the house-accompanying pits as the actual investigation targets are given. Second, the physical background, the applied measurement methods and our approach for the determination of the Koenigsberger ratio are explained. Then, we present the inversion results for one drilling profile in detail and a comparative overview including five more profiles. In addition, the results of the laboratory analyses of the samples are given. In the discussion section, we first examine methodical aspects and then give an interpretation regarding the magnetic history of the site.

2 | THE ARCHAEOLOGICAL SITE OF VRÁBLE 'FARSKÉ'

2.1 | General information

The site of Vráble (Slovakia) is located in the valley of the upper Žitava River, one of the many north–south running tributaries of the Danube. At about 140 m above sea level (a.s.l.), the site is situated in a slightly hilly environment on fertile soils developed on a loess plateau above the river. Research at this site started in 2009 with large-scale magnetic prospections and excavations as well as geoarchaeological research were conducted in ensuing years (Dreibrodt, Furholt, Hofmann, Hinz, & Cheben, 2017; Furholt et al., 2014; Müller-Scheeßel, Cheben, Filipovic, Hukelová, & Furholt, in press). They have shown that the site actually consisted of three co-existent settlements (see Figure 1) of the Linearbandkeramik (LBK). Each settlement encompassed a size of 10 to

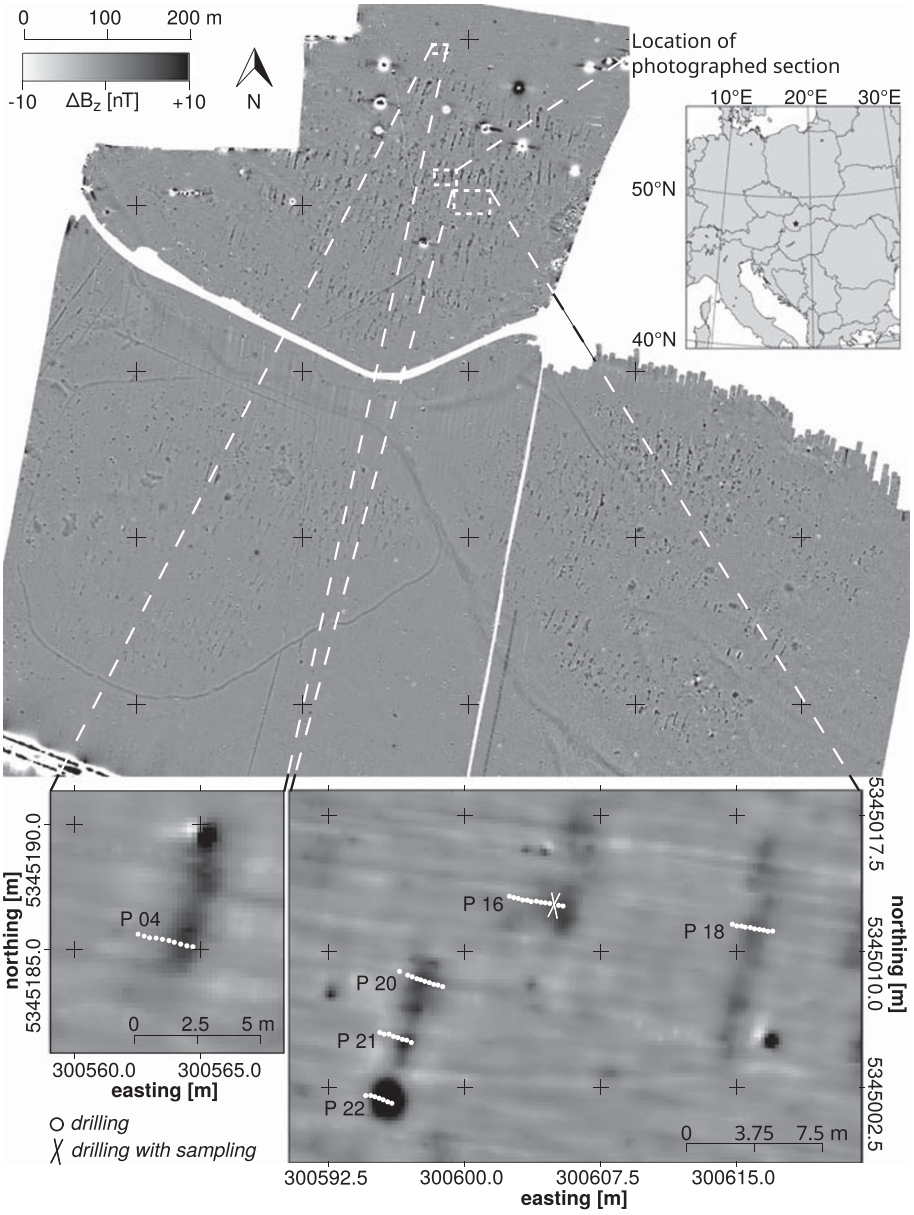

FIGURE 1 Magnetic map of the site Vráble and its location in Slovakia (upper right inlet). The detailed views show the location of the drilling profiles with the single drillings marked with a white dot. From one drilling (marked with a cross), samples were taken and analysed in the laboratory

15 ha and, at their peak, they probably incorporated up to 60 houses with about 500 inhabitants (Müller-Scheeßel et al., 2020). The settlements of Vráble as a whole date between ca 5250 and 4950 cal BCE (Meadows, Müller-Scheeßel, Cheben, Rose, & Furholt, 2019) and belong to the late local phase of the LBK (Želiezovce group) (Furholt et al., 2014).

2.2 | Characteristic of house-accompanying pits

The house-accompanying pits usually run along the full length of both sides of the respective houses (10–30 m). They measure about 2–3 m in width and their bottom is 0.8–1.5 m below today's surface. The varying depth of the bottom may point to the fact that they were dug out in sections and not in one go. The microtopography was also documented with electromagnetic induction (EMI) and ground-penetrating radar (GPR) measurements on the stripped surface (approximately 60 cm below the present surface) during the course of an excavation (Pickartz et al., 2020). Measurements were conducted with a GSSI 400 MHz antenna and GF Instruments CMD Mini Explorer in vertical and horizontal coplanar orientation. The GPR reflection of the bottom of the pit was correlated with a conductivity in the inverted EMI conductivity distribution. The isosurface of this conductivity value is interpreted as the three-dimensional image of the pit bottom. In most instances, the fill of the pits is very homogeneous and consists of dark brown soil (Munsell colour 10YR3/3–3/4), mixed with a few archaeological finds like ceramics, stone tools and animal bones (Figure 2). In many cases towards the top, but sometimes also near the bottom, a thin layer consisting of a higher amount of daub is found. However, as seen in Figure 1 these layers do not always produce a distinctly strong signal to be characterized as (thermo-)remanent feature. Divergent fillings, especially encountered at the southern ends, like checkered or ashy soil might point to special activities having taken place there.

It is usually taken for granted that the long pits flanking LBK houses were used as clay extraction pits and subsequently filled with waste, whereas their function and the filling processes are still debated (Kvetina & Rídký, 2017; Wolfram, 2013). However, recent research (Allard et al., 2013) as well as our own excavations (Müller-Scheeßel et al., in press) have shown that the debris is patterned and thus obviously reflects activities having taken place during the existence of the respective house. Therefore, we expect that material coming from undisturbed layers of lateral pits belong to the accompanying house.

3 | PHYSICAL BACKGROUND AND METHODS

In this section, we present first the theoretical framework for this study, followed by a description of the methods for data acquisition in the field and laboratory. Finally, we present the inversion algorithm that we used to estimate the Koenigsberger ratio.

3.1 | Physical background

Magnetic anomalies mapped in archaeological prospection arise from spatial variations of the 'total' magnetization of the soil $\vec{M_T}$. The total magnetization is the sum of a remanent $\vec{M_R}$ and induced $\vec{M_I}$ component:

$$\vec{M_T} = \vec{M_R} + \vec{M_I} \tag{1}$$

$$= \vec{M_R} + \kappa \cdot \vec{H}, \tag{2}$$

where κ denotes the isotropic volume susceptibility and $\vec{H}$ the vector of the ambient earth's magnetic field. The Koenigsberger ratio is the ratio of remanent to induced magnetization

$$Q = \frac{|\vec{M_R}|}{|\vec{M_I}|} \tag{3}$$

and is independent of the magnetization directions.

The magnetic susceptibility can be measured at different frequencies of an artificially generated exciting magnetic field to determine the frequency dependence of the material (Kainz & Cotter, 2018).

FIGURE 2 Photogrammetry of a section of the eastern long pit of house 245 (trench 8, 2014). The pit is composed of several layers with humous material and inclusions of daub and pottery [Colour figure can be viewed at wileyonlinelibrary.com]

The device used in the present study, a MS3 with MS2B sensor by Bartington Instruments Ltd (Witney, United Kingdom), is an inductor coil instrument that is tuned to resonance. Hereby, the relative permeability μ_r of the sample modulates the frequency of oscillation (Evans & Heller, 2003). It is related to the magnetic susceptibility by

$$\kappa = \mu_r - 1. \quad (4)$$

The magnetic grain size distribution can be investigated by measuring the susceptibility at two (or more) different frequencies in the laboratory. The used device performs low-frequency measurements κ_{lf} at 0.465 kHz and high-frequency κ_{hf} measurements at 4.65 kHz. From this data the frequency dependent susceptibility is computed in percentage by

$$\kappa_{fd} = (\kappa_{lf} - \kappa_{hf})/\kappa_{lf} \times 100\% \quad (5)$$

which is correlated with the grain size distribution.

3.2 | Data acquisition

3.2.1 | Magnetic field measurements

Between 2010 and 2012, the area of the site Vráble was extensively surveyed (Furholt et al., 2014) by the Romano-Germanic Commission of the German Archaeological Institute. The surveys were conducted with the FGM650 gradiometers by Sensys GmbH (Bad Saarow, Germany) in a 16-sensor array. The distance between the lower and upper sensor is 65 cm. In the array, the sensors have a distance of 25 cm cross-line and are mounted 35 cm above the ground. The survey speed of 12 km/h to 16 km/h results in in-line point distances of 30 cm with a sample rate of 20 readings per second.

Each magnetic profile was filtered with a third-order Butterworth low-pass filter (cut-off wavenumber at 0.5 m^{-1}) to remove short-wavelength random noise and apply a gentle smoothing. Also the linear trend was removed from each profile.

3.2.2 | Field susceptibility measurements

The drilling points were placed along linear profiles crossing the house accompanying pits orthogonally with a spacing of 25 cm (Figure 1). The boreholes were drilled with an auger corer of 22 mm diameter to a maximum depth of 2 m (if feasible). For the susceptibility measurements we used the MS3 device by Bartington Instruments Ltd in combination with the MS2H sensor operating with a frequency of 1.3 kHz. Starting at a depth of 10 cm, the probe was lowered in 5 cm steps to the maximum depth of 2 m or until no further lowering was possible. For each hole, the measurements were preceded and followed by drift measurements in the air. Each susceptibility depth curve was manually edited to remove a systematic increase of the susceptibility in the depth range from 1.00 m to 1.15 m because of soil compaction due to drilling. In addition, the topsoil susceptibility was measured with the same device using the MS2K sensor (operating frequency: 0.93 kHz) at the selected drilling points. The susceptibility values of the topsoil were averaged along the profile and the resulting mean value was attributed to the uppermost 10 cm of the soil column.

3.2.3 | Sediment analyses

To characterize the sediments under investigation and elucidate the possible sources of magnetization, samples from drill location P16_175 (Figure 1) were taken for additional laboratory analysis. The following paragraphs describe the methods that were used to characterize the sediment with laboratory analysis.

3.2.3.1. Sample preparation

Samples were taken in the field from the auger corer (P16_175, see Figures 1 and 7). Because of the small diameter of the corer (22 mm), sample material had to be gathered over depth intervals of 20 to 30 cm in order to provide sufficiently large soil volumes for the laboratory analysis. Some material was lost or displaced during the coring process. All samples were dried at 35 °C for at least 3 weeks and disintegrated with mortar and pestle. Following standard procedures of pedology and geoarchaeology, the fraction > 2 mm was separated via dry sieving.

3.2.3.2. Laboratory susceptibility measurements

The magnetic susceptibility was measured on 10 ml of the < 2 mm, homogenized samples using a MS3 meter by Bartington Instruments Ltd with the MS2B probe. Measurements were carried out at both low (0.465 kHz) and high (4.65 kHz) frequency. A reference sample consisting of 1% iron(II,III) oxide (Fe_3O_4, magnetite) was measured repeatedly and the samples' susceptibility values were calibrated using this reference before converting them to mass-specific susceptibility. Finally, low and high frequency measurements were used to calculate the percentage of frequency dependent susceptibility (see section 3.1). The measurements were repeated with the whole sample – including particles > 2 mm – to check their influence on the values and ensure comparability with field measurements.

3.2.3.3. Iron content

The content of dithionite soluble iron (Fe_d) indicating the formation of goethite and maghemite/magnetite during soil formation processes was determined according to (Blakemore, Searle, & Daly, 1987). Via this method a reducing reactant ($Na_2xtS_2O_4$) at a stable pH-value dissolves non-crystalline to badly crystalline oxides of iron, and their concentration was measured using atomic absorption spectroscopy in the supernatant. The dithionite soluble fraction of iron is typical for products of soil formation processes.

3.2.3.4. Soil colour

The colour of the samples was measured using a Voltcraft Plus RGB-2000 Colour Analyser (Wollerau, Switzerland) set to display in a ten-bit red, green, and blue (RGB) colour space (Rabenhorst et al., 2014; Sanmartín, Chorro, Vázquez-Nion, Martínez-Verdú, & Prieto, 2014). This digital device has integrated light-emitting diode (LED) lighting and an external sensor with a 45/0 measuring geometry to ensure the minimization of specular reflection. It has a spectral range of 400 to 700 nm and measures with a precision of < 3 for the RGB colour model. In this system red, green, and blue vary from 0 to 1023 with 0, 0, 0 representing black and 1023, 1023, 1023 representing white.

3.2.3.5. X-ray fluorescence (XRF)

The total elemental content of the samples was measured with a portable electron dispersive (PED)-XRF device (Niton XL3t900-ed-XRF by Thermo Fisher Scientific, Waltham, Massachusetts, USA). For this purpose the < 2 mm fraction was first homogenized in an Agate mill and then placed in a plastic tube covered by a 4 μm film. These were then measured in a lead-mantled measurement chamber with He-flotation using the "mining, Cu/Zn" settings for 300 s. The instrumentally determined values for iron (Fe), manganese (Mn), titanium (Ti), calcium (Ca), potassium (K), silicon (Si), aluminium (Al), phosphorus (P), zirconium (Zr), strontium (Sr), and rubidium (Rb) were finally corrected using the equations published byDreibrodt et al., 2017.

3.2.3.6. X-ray diffraction (XRD)

The mineral assemblage of the samples of core P16_175 was studied by XRD measurements using a Philips (Amsterdam, Netherlands) diffractometer PW1710 (Cu radiation, 40 kV, 25 mA). Conventional powder samples were measured on ground samples of the fine earth fraction < 2 mm ($2 \cdot \vartheta$: 2 to 80, step size: 0.02, time: 2 s).

3.2.3.7. Loss-on-ignition (LOI)

LOI values were measured to estimate the organic matter and carbonate contents of the sediments (Dean, 1974). First the samples were dried at 105 °C overnight. The contents of organic matter and carbonates were then determined from the weight losses caused by heating the samples for each 2 h at 550 °C and 940 °C, respectively. Finally, the LOI values were converted into contents of soil organic matter and carbonates based on empirically determined site specific factors by linear regression.

3.3 | Magnetic data interpretation

The next sections describe the components of the magnetic data interpretation. The interpretation starts with model calculations assuming solely induced magnetization and the susceptibility distributions determined *in situ*. The resulting synthetic data deviate strongly from the measured magnetic field data, which motivated the introduction of a model for remanent magnetization. Based on this model a representative Koenigsberger ratio is finally determined with an inversion calculation for each profile.

3.3.1 | Magnetic forward calculation

To determine the portion of the magnetic anomalies that is caused by induced magnetization we performed magnetic model computations based on two-dimensional subsurface susceptibility models such as sketched in Figure 3. The subsurface below the drilling profile is divided in a regular grid with 0.125 m horizontal and 0.05 m vertical cell size. Between two drilling locations the susceptibility data are interpolated and smoothed. To avoid a boundary effect from the bottom model boundary, the susceptibility values were tapered with a cosine to zero. This extends the model to 3.0 m depth. To avoid boundary effects from the sides of the drilled section we extrapolated the susceptibility depth curves of the two outermost drilling locations to the sides and tapered them to an average susceptibility depth curve. This background curve represents the arithmetic mean of

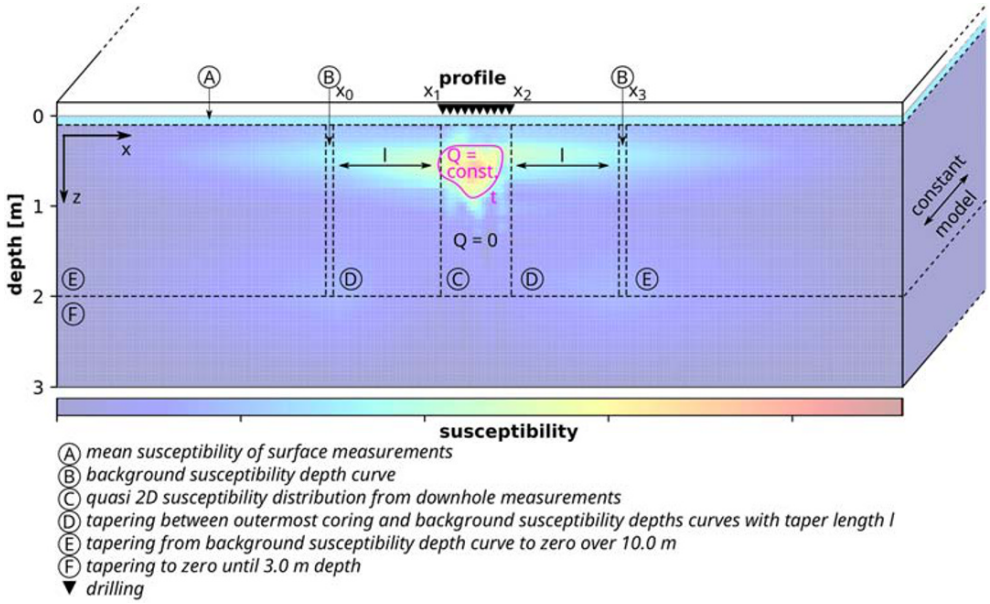

FIGURE 3 Sketch of a susceptibility model with the three inversion parameters *Q* (Koenigsberger ratio), *t* (threshold) and *l* (taper length) [Colour figure can be viewed at wileyonlinelibrary.com]

curves measured outside the pits in surrounding undisturbed soils (Figure 4(b)). The length of the horizontal tapering interval l was held variable and tuned later by the inversion computation. Finally, to avoid boundary effects from the sides of the model, the susceptibility depth curve of the background was tapered to zero over a length of 10.0 m.

The forward calculations were carried out in Python using the library 'Fatiando a Terra' (Uieda, Oliveira, & Barbosa, 2013). From this package we used the implementation of the formula by Plouff (1976) for each model cell to calculate the difference in the vertical component of the resulting magnetic field $\Delta B_z^{syn,i}$ as measured by the differential fluxgate sensors at each observation point i = 1,...,N. For the modelling we applied the orientation and field strength of the present ambient earth magnetic field according to the 'International Geomagnetic Reference Field' (IGRF) as described by Thébault et al. (2015), i.e. the following values: declination D = 3.87°, inclination I = 64.63° and magnetic field strength B = 48626.3 nT.

3.3.2 | Remanent magnetization model

To determine the remanent soil magnetization in a representative way, we assumed that the Koenigsberger ratio is an unknown constant along each profile, the value of which is to be determined by the inversion calculation (see section 3.3.3). The remanent magnetization is thought to occur only above an unknown threshold t in

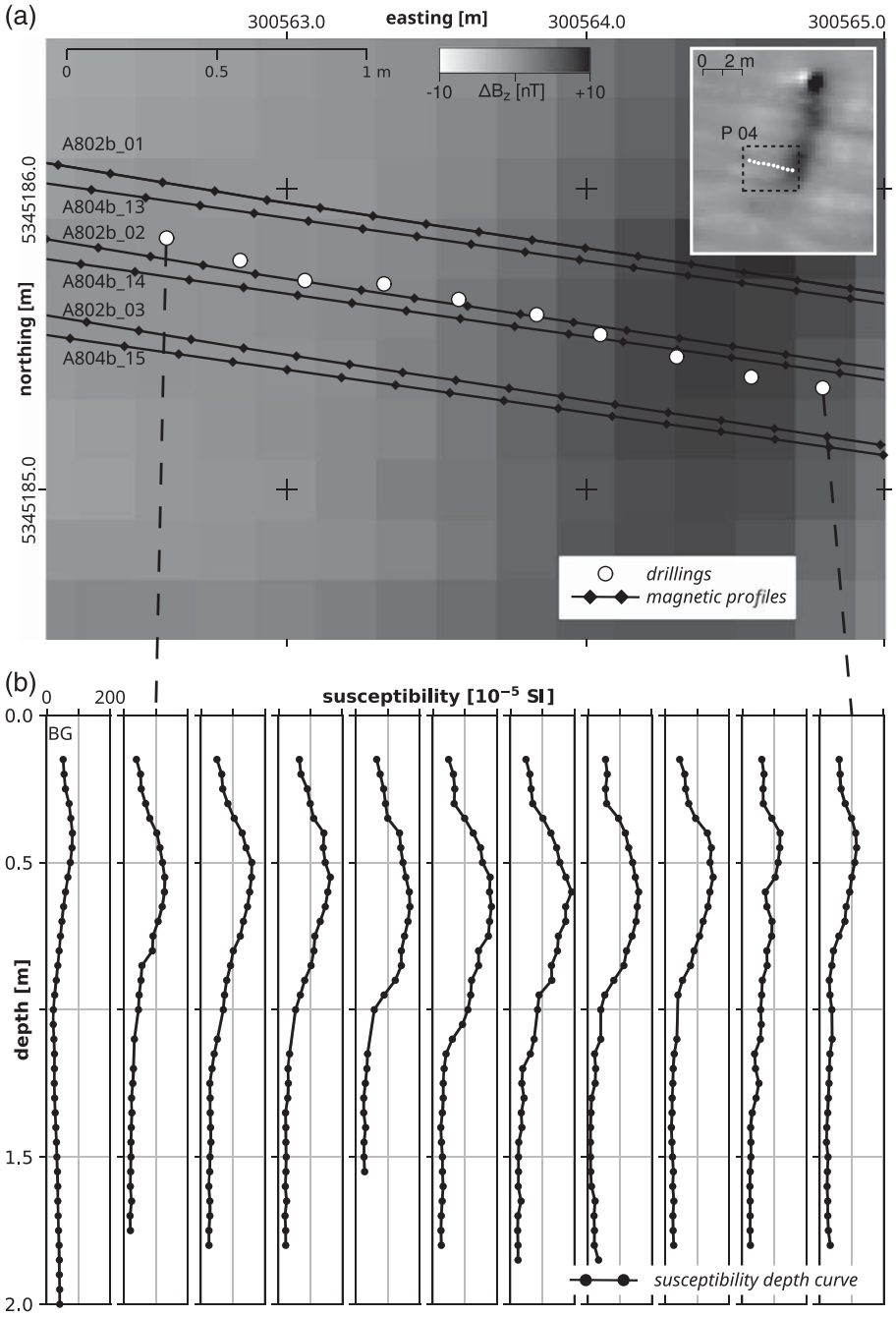

FIGURE 4 (a) Close-up of profile P04 with the location of the drilling points and the magnetic sensor traces that were chosen for the inversion. (b) The left column (BG) shows the average 'background' susceptibility depth curve. The remaining columns show the measured susceptibility depth curves of profile P04

the measured susceptibility (see Figure 3), where the numerical value of the threshold would again be determined by inversion computation. This concept was implemented by defining trial values for the threshold and by attributing remanent magnetization only to grid cells with a measured susceptibility above these thresholds. By applying this threshold we imply that the surrounding loess matrix has a negligible remanent magnetization compared to the filling of the pits.

As to the orientation of the remanent magnetization vector, we assume that the change in the orientation of the ambient magnetic field since the filling of the pits is neglectable with respect to the resolution of the inversion computation. Indeed, palaeomagnetic studies have shown that the deviation between the declination during the settlement time at the end of the sixth millennium BCE and the recent declination is of the order of five only (see Figure 8 based on Pavón-Carrasco, Osete, and Torta (2010)). Therefore, we applied the orientation of the recent earth's magnetic field according to the IGRF. This simplification is justified by a synthetic model study that is presented in Appendix B.

3.3.3 | Inversion of magnetic field data

We invert the magnetic data of each profile with respect to three variables: a representative constant Koenigsberger ratio Q, a susceptibility threshold t identifying the remanently magnetized cells and the length of the horizontal tapering interval l limiting the extrapolation of the drilled section to the sides. The inversion is performed by least-squares fitting of synthetic to field data.

To describe the horizontal tapering outside the drilled profile, let x_1 and x_2 be the location of the outermost left and right downhole measurement. Moreover, let x_0 and x_3 describe the locations of the background susceptibility depth curve $\kappa_{BG}(z)$, so that $x_1 - x_0 = x_3 - x_2 = l$ (see Figure 3). Then, the taper $f(x)$ along the profile x is

$$f(x) = \begin{pmatrix} \cos\left(\frac{l-(x-x_0)\pi}{l\ 2}\right), & \text{for } x_0 \le x \le x_1 \\ \cos\left(\frac{(x-x_2)\pi}{l\ 2}\right), & \text{for } x_2 \le x \le x_3. \end{pmatrix} \quad (6)$$

The susceptibility distribution for $x_0 \le x \le x_1$ and $x_2 \le x \le x_3$ is then

$$\kappa(x,z) = \begin{pmatrix} \kappa(x_1,z) + (\kappa(x_1,z) - \kappa_{BG}(z)) \cdot f(x), & \text{for } x_0 \le x \le x_1 \\ \kappa(x_2,z) + (\kappa(x_2,z) - \kappa_{BG}(z)) \cdot f(x), & \text{for } x_2 \le x \le x_3. \end{pmatrix} \quad (7)$$

As described in section 3.3.1, the subsurface is divided into a regular grid where $\kappa_j = \kappa(x_j, z_j)$ denotes the susceptibility in cell $j = 1,\ldots,M$ at location (x_j, z_j). The calculated magnetic gradiometer data at observation point i resulting from solely induced magnetization is

$$\Delta B_z^{ind,i} = \sum_{j=1}^{M} a_{ij}\kappa_j, \quad (8)$$

where a_{ij} is a factor that comprises the information about the relative location of sensors and cells, the earth magnetic field as exciting field and the cell size (Plouff, 1976). Introducing remanent magnetization described by the Koenigsberger ratio Q and occurring only in cells with a susceptibility larger than the threshold t ($\kappa_j > t$), extends Equation 8 to

$$\Delta B_z^{syn,i} = \sum_{j=1}^{M} a_{ij}\kappa_j + Q \cdot \sum_{j=M_t+1}^{M} a_{ij}\kappa_j. \quad (9)$$

We here assume that the cells are in the order from smallest $\kappa_{j=1}$ to highest susceptibility $\kappa_{j=M}$ and that κ_{M_t} is the largest susceptibility value smaller than t.

For $t,l = 0$, Equation 9 describes an over-determined system of linear equations for Q. However, for $t,l \neq 0$ Equation 10 describes a non-linear system with inversion parameters in the summation index (M_t) and the underlying subsurface model (l).

In least squares sense, the cost function is

$$L(Q,t,l) = \sum_{i=1}^{N} \left(\Delta B_z^{obs,i} - \Delta B_z^{syn,i}(Q,t,l)\right)^2 0 \le Q \quad 0 \le t \quad 0 \le l \le l_{max}. \quad (10)$$

Hereby, all three parameters are constraint to be positive. Moreover, l is bound to be smaller than the distance to the next obvious magnetic anomaly on the profile l_{max}. This is always in a few metre distance.

To solve this non-linear optimization problem, we applied a subspace trust region interior reflective (STIR) algorithm (Branch, Coleman, & Li, 1999). The idea of a trust region algorithm is to approximate the cost function in a region around the start parameters resp. the current solution of the iterative process. The approximation is then minimized in this trusted region, which is the so called subproblem. The used algorithm restricts the subproblem to two dimensions, in which s_1 and s_2 span the subspace. The first direction s_1 is determined by the conjugate gradient, the second s_2 either by the direction of a Newton step or a negative curvature vector. If the solution of the subproblem leads to a smaller value of the cost function, this step is accepted and a new current solution is found. Otherwise the trust region is shrunk and all steps are repeated. The complete procedure is iteratively repeated until convergence. The evaluation of the inversion results by means of two different approaches is discussed in Appendix A.

4 | RESULTS

In the first subsection we present the results of the inversion of magnetic field data in two steps: first for one exemplary profile in detail and, next, for the remaining five profiles in form of an overview and table. In the second subsection, we include the results of the laboratory analyses of the samples.

4.1 | Results of the inversion of magnetic field data

4.1.1 | Example profile 4

Figure 4(b) shows the susceptibility depth curves that were measured along profile P04 and are the base for the interpolation and extrapolation of the two-dimensional susceptibility distribution. The susceptibility distribution is shown in Figure 5(b) with the observed and calculated magnetic data at the top (Figure 5(a)). The left column of Figure 4(b) shows the mean curve for the subsurface outside of archaeological features ('background', 'BG'). The different magnetic profiles that were used for the inversion of the drilling profile P04 are shown in Figure 4(a). These are the measurements of single sensors in the gradiometer array

For the uppermost layer of the topsoil (0.0–0.1 m depth) no data from borehole measurements are available. Therefore, we assumed a mean susceptibility of 74.5×10^{-5} SI for this uppermost part of the surface layer, which is the average of the surface measurements. Susceptibility values deeper than 10 cm were determined *in situ* (cf. Figure 4). Between 10 cm and 30 cm depth we found comparatively small susceptibility values between 60 and 70×10^{-5} SI, which show only little lateral variation and represent the values of the topsoil mixed by plowing. The susceptibility distribution of the subsoil shows increased values up to 192×10^{-5} SI found in the central part in 60 cm depth. Below this maximum the susceptibility values decrease to around 25×10^{-5} SI. Measurements outside the pits suggest that the susceptibility values around 150×10^{-5} SI can be used as an approximate indicator for the boundary between pit and surrounding soil matrix (see also Figure 4). Using this criterion the pit cross-section turns out to be a wide-angled V-shape. The top of the pit is found in about 50 cm depth where it is approximately 150 cm wide. The bottom of the pit reaches down to about 75 cm depth. The centre of the pit shows the highest susceptibility values.

The measured magnetic anomaly has a maximum of 7.2 nT and a half-width of approximately 1.8 m. Assuming solely induced magnetization, the calculated magnetic data reach a maximum of 1.6 nT (dotted line, Figure 5). This corresponds to only 22% of the observed value or a maximal difference of 5.6 nT at the peak.

The difference along the profile between the measured and calculated magnetic anomaly can only be explained with a significant remanent magnetization. However, test computations have shown that an optimum fit cannot be reached by simply enhancing the susceptibility values of the model by a factor of Q. As shown in Figure 6 the fit improves if a lateral taper with adjustable width l is applied, which serves to grade susceptibility distribution from the pit to the undisturbed surrounding sediment. Obviously, also this additional condition is not sufficient for obtaining a satisfactory fit because the shape of the anomaly function is still not well reproduced in the boundary areas. This can be improved by introducing a threshold that restricts the application of a $Q > 1$ only to soil volumes exceeding a certain minimum susceptibility t. Figure 6 shows that the combination of Q and t is not sufficient as t is basically set to 0 SI by the inversion. The introduction of the variable horizontal taper l is primarily a numerical trick. However, it can be justified by the interpretation that the upper portions of the pit fill may have been smeared to a certain extent to outside the pit by agricultural activity in the past millennia.

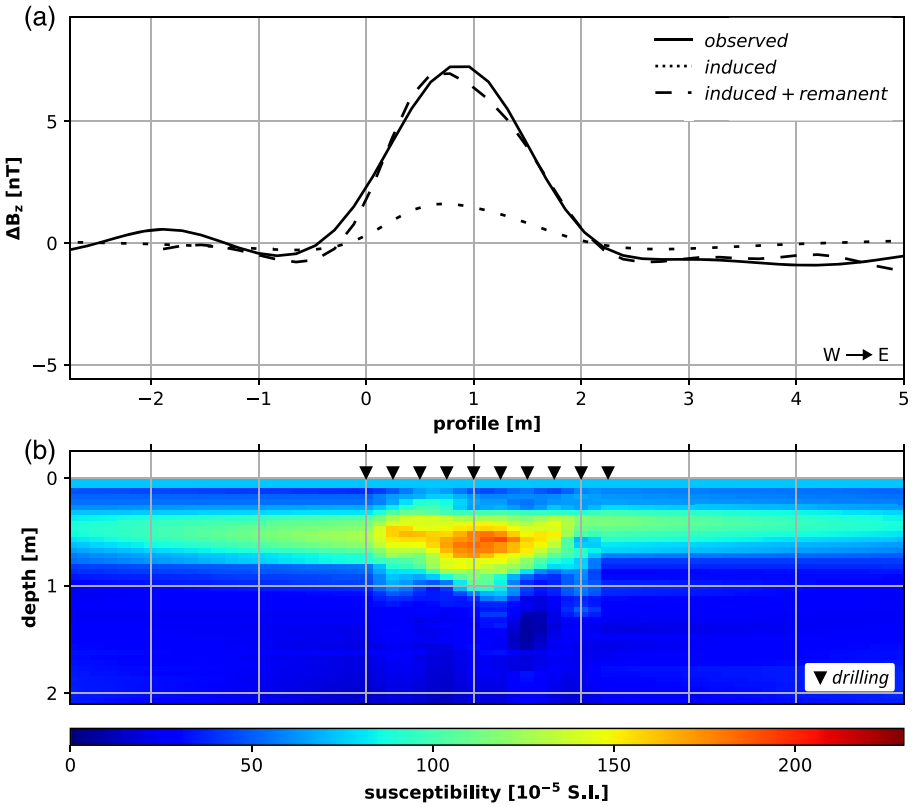

FIGURE 5 Profile P04. (a) Measured magnetic profile (vertical component gradiometer data, A802b_03, see Table 2 and Figure 4) and calculated magnetic anomaly assuming induced (dotted line) and induced plus remanent (dashed line) soil magnetization. The dashed line shows the optimum fit obtained for a Koenigsberger ratio Q of 2.4 for subsurface points with a susceptibility $\kappa \geq 90 \times 10^{-5}$ SI, and $Q = 0$ elsewhere. The underlying two-dimensional susceptibility distribution is shown in (b). Downhole measurements of magnetic susceptibility were performed at the drilling locations indicated by black triangles (cf. Figure 4). Outside this area the values were extrapolated and tapered to the average κ-depth function of the surrounding soil [Colour figure can be viewed at wileyonlinelibrary.com]

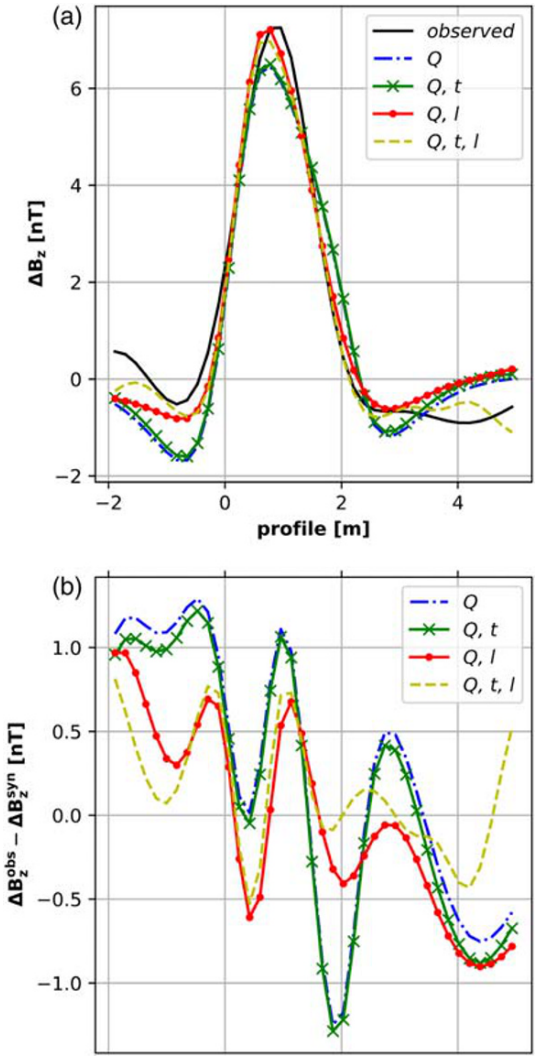

FIGURE 6 (a) Comparison between observed magnetic anomaly and calculated anomalies with different sets of parameters for profile P04 (cf. Figure 5). All model parameters (Koenigsberger ratio *Q*, threshold *t* and taper length *l*) are tuned by the inversion to optimum fit. (b) Difference between the observed magnetic anomaly and the different model responses [Colour figure can be viewed at wileyonlinelibrary.com]

This soil movement assumingly has removed VRM since it disturbed the orientation of the magnetic particles.

4.1.2 | Comparison of different magnetic profiles

The results of all drilling profiles are shown in Figure 7. They differ in both, the appearances of the cross-sections of the pits and the related magnetic anomalies. Yet, the underlying susceptibility-depth functions are very similar in their general form: the susceptibility increases until a maximum is reached and then decreases down to around 25×10^{-5} SI. The location and amplitude of the maximum as well as the slope determine the cross-section of the pits.

Table 1 shows the statistical evaluation (A) of all drilling and magnetic profile combinations. These cases do not depend on the drilling profile but rather on the magnetic profile. For the majority of profile combinations the cost functions have a well-defined minimum for *Q*. Exceptions of this are profiles 16 and 21, which show considerable trade-offs between the inversion variables.

The best fitting model parameters in terms of root mean square (RMS) errors are shown in Table 2. The arithmetic mean for each drilling profile according to the statistical evaluation (B) is also given in Table 2. A comparison of Tables 1 and 2 shows that the expected values and the best fitting values are very similar to each other.

The mean Koenigsberger ratio varies between 1.8 ± 0.2 and 7.0 ± 3.3, in which the mean of all best fitting values is 3.3 ± 2.2. The mean threshold in the susceptibility values, over which remanent magnetization is considered, varies between $27 \pm 3 \times 10^{-5}$ SI and $160 \pm 31 \times 10^{-5}$ SI with an overall mean of $78 \pm 54 \times 10^{-5}$ SI. Considering all best fitting values for the threshold, clusters at approximately 20–30 $\times 10^{-5}$ SI and 90–110 $\times 10^{-5}$ SI are found.

4.2 | Sediment analyses

In this section, we present the laboratory analyses of the samples from core P16_175. This core is part of profile P16 (cross in Figure 1) and was sampled to analyse the sediment layer below the loess. The laboratory analyses enable to investigate the causes of susceptibility and remanent magnetization. The samples are mixed samples, which were taken from the Auger corer from 20 to 35 cm long depth intervals.

According to field grain size estimations (Eckelmann et al., 2006), the sediment of the upper 164 cm (surface soil, pit fill, loess) could be classified as loamy silt (Ut2). The sediment in a depth of 164 to 200 cm is a silty sand (Su2), probably exhibiting a periglacial slope debris layer. The two upper samples were taken from 0.20 to 0.40 m and 0.53 to 0.85 m depth. They are representative for the top soil and the uppermost pit-fill, which consist only of grains < 2 mm. The two deeper samples are from 1.13 to 1.44 m and 1.64 to 2.00 m depth. In addition to the small-grained fraction they also contain a fraction > 2 mm. The fraction > 2 mm of the sample from 1.13 m to 1.4 m depth contains daub and gravel. The sample from 1.64 m to 2.0 m has a small gravel content. The susceptibility was measured on the fraction < 2 mm to be comparable to standard pedological samples as well as on the complete samples to be comparable to the *in situ* measurements. All other laboratory analyses were solely conducted on the fraction < 2 mm.

Figure 8 shows the results of the different laboratory analyses and, for comparison, the downhole measurements of the susceptibility. Qualitatively the downhole (Figure 8(a)) and laboratory (Figure 8(b)) measurements show the same trends of susceptibility with depth. This trend shows the highest susceptibility values around 60 cm depth and a decrease below as described already in section 4.1.1. For comparison the downhole measurements are also shown in Figure 8(b). Some material has been lost during coring and therefore, the sediments might have shifted in the corer. In general, the volume susceptibility measurements in the laboratory show

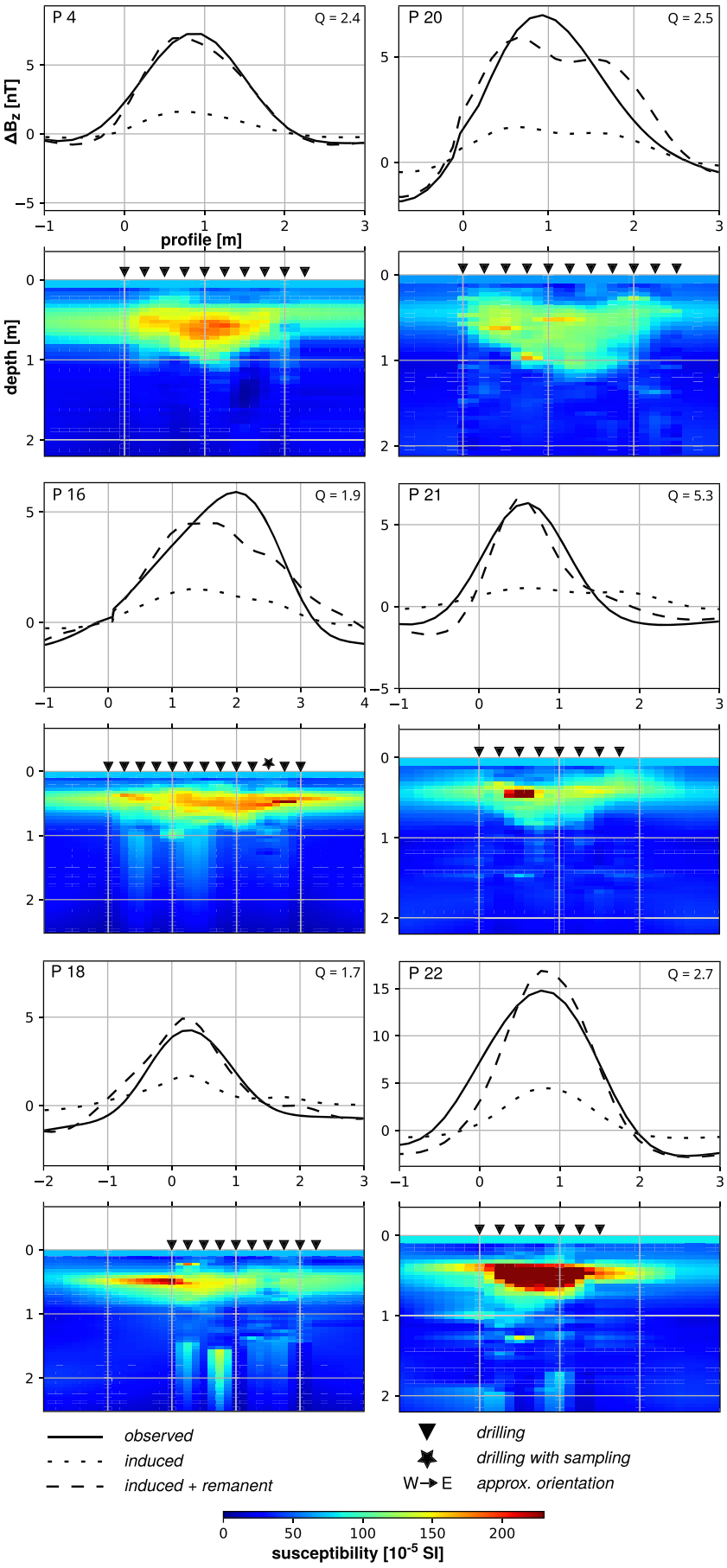

FIGURE 7 Data of all drilling profiles with the magnetic profiles (observed, induced and induced plus remanent) as line plots (uneven rows). Beneath the magnetic data, the measured susceptibility distributions (even rows) are shown with the drilling locations marked as triangles [Colour figure can be viewed at wileyonlinelibrary.com]

TABLE 1 Expected model parameters with standard deviation for every drilling and magnetic profile combination.

Profile	Magnetics	<Q>	σ_Q	σ_Q (%)	<t> (10^{-5} SI)	σ_t (10^{-5} SI)	σ_t (%)	<le (m)	σ_l (m)	σ_l (%)
P04	802b_01	1.9	0.1	5.4	107	7	6.4	2.5	0.8	31.1
P04	802b_02	2.7	0.1	5.0	100	4	3.7	4.5	0.6	14.2
P04	802b_03	2.4	0.1	2.8	90	3	3.8	3.6	0.1	2.8
P04	804b_13	2.5	0.1	5.5	97	10	10.7	3.8	0.7	17.6
P04	804b_14	3.3	0.4	12.3	53	25	47.0	4.5	0.2	3.8
P04	804b_15	2.7	0.1	2.8	95	12	13.1	4.4	0.5	11.4
P16	657b_07	1.9	> 0.1	0.9	90	1	1.1	1.9	> 0.1	2.3
P16	657b_08	2.0	> 0.1	2.4	23	4	15.6	0.7	0.4	54.3
P16	657b_09	2.7	> 0.1	0.9	22	> 1	2.3	1.5	> 0.1	3.2
P16	657b_10	2.7	> 0.1	0.9	22	> 1	2.3	1.5	> 0.1	2.8
P16	657b_11	3.0	> 0.1	0.2	28	> 1	0.1	2.0	> 0.1	0.4
P18	657b_07	1.5	0.1	5.7	60	2	3.1	1.7	> 0.1	1.0
P18	657b_08	1.7	> 0.1	2.8	113	3	2.4	1.8	0.1	4.2
P18	657b_09	1.8	> 0.1	2.5	113	2	1.7	1.9	0.2	10.2
P18	657b_10	1.9	> 0.1	0.5	114	> 1	0.4	2.3	> 0.1	> 0.1
P18	657b_11	1.9	> 0.1	2.1	115	4	3.8	2.0	0.2	7.9
P20	658b_01	3.5	> 0.1	> 0.1	107	> 1	> 0.1	7.6	0.1	1.4
P20	658b_02	2.7	> 0.1	1.2	74	1	1.0	1.3	0.1	5.9
P20	658b_03	3.6	> 0.1	0.5	2	1	53.0	0.0	> 0.1	117.8
P20	658b_04	2.5	0.1	5.7	4	13	348.7	0.2	0.7	470.5
P20	658b_05	2.5	0.1	2.2	2	2	149.1	0.0	> 0.1	75.8
P21	661b_06	4.2	3.3	78.2	149	32	21.2	3.9	0.3	8.1
P21	661b_07	6.8	3.7	54.3	157	32	20.2	0.7	0.6	83.6
P21	661b_08	10.2	0.9	9.0	181	21	11.5	0.2	0.3	168.0
P21	661b_09	10.9	1.6	14.6	186	21	11.4	0.2	0.3	226.7
P21	661b_10	11.2	1.8	16.3	181	20	11.1	0.3	0.4	117.4
P22	662b_07	2.7	> 0.1	1.4	30	1	2.2	1.1	0.1	7.2
P22	662b_08	3.7	0.1	2.2	25	1	3.2	1.1	0.1	8.8
P22	662b_09	3.7	> 0.1	0.3	23	> 1	1.8	1.1	> 0.1	> 0.1
P22	662b_10	3.9	> 0.1	0.2	27	> 1	0.3	1.4	> 0.1	0.1
P22	662b_11	3.6	> 0.1	0.2	28	> 1	1.3	1.4	> 0.1	> 0.1

somewhat lower values than the field measurements. This can be explained with the preparation process, in which the samples are decompacted on the way from the drilling to the laboratory measurements. Therefore, laboratory and *in situ* densities and related volume susceptibility values of the soil may be somewhat different. The laboratory measurements include also a sample from below 1.5 m depth, which shows again increased susceptibility values.

Figure 8(b) shows the high and low frequency measurements of the complete samples *versus* the ones of the fraction < 2 mm. For the sample in 1.13–1.44 m depth, the complete sample shows higher susceptibility measurements whereas for the sample in 1.64 m to 2.0 m depth it is vice versa. This is explainable by the detected daub inclusions in sample 1.13–1.44 m

The frequency dependent portion of susceptibility (Figure 8(c)) is approximately 9% for the two uppermost samples and decreases over 6% down to 0.1% for the deepest. Even though the high and low frequency measurements of the fraction < 2 mm and the complete sample for the two deepest samples differ in their absolute values, the resulting frequency dependent susceptibility values are similar.

The trend of the total iron content by weight (Figure 8(d)) is similar to the trend of the susceptibility except for the deepest sample. The susceptibility value of the deepest sample is the highest measured one, however the iron content in this sample is the lowest measured one. This ratio points to the presence of iron compounds in the deepest sample with a higher susceptibility than the iron compounds in the other samples.

The XRD mineral assemblage shows small differences between the samples. They consist of quartz, feldspars, mica, with higher amounts of expandable clay minerals in the upper two samples. Spurs of maghemite/magnetite, gypsum and calcite (lower two samples) are present as well. The Fe_d/Fe_t ratios are the highest in the upper two

TABLE 2 Inversion results of the drilling profiles with mean Koenigsberger ratio $\bar{Q}$, mean threshold $\bar{t}$ and mean taper length $\bar{l}$ based on the best fitting inversion results per magnetic profile, that are given in the second half of the table with the respective root mean square (RMS) error

Drilling profile	$\bar{Q}$	$\bar{t}$ (10^{-5} SI)	$\bar{l}$ (m)	Magnetic profile	Q	t (10^{-5} SI)	l (m)	RMS (10^{-1} nT)
P04	2.3 ± 0.3 (14.8%)	101 ± 6 (6.3%)	3.9 ± 0.9 (22.8%)	A802b_01	1.9	105	2.9	5.4
				A802b_02	2.7	102	4.9	5.0
				A802b_031	2.4	89	3.7	3.8
				A804b_13	2.6	105	4.6	5.0
				A804b_14	2.5	98	4.4	6.5
				A804b_15	1.9	105	2.9	5.4
P16	2.0 ± 0.1 (4.7%)	49 ± 37 (75.3%)	1.1 ± 0.7 (64.5%)	A657b_07	1.9	90	1.9	8.6
				A657b_081	1.9	90	1.9	8.6
				A657b_09	2.1	23	0.6	8.8
				A657b_10	2.0	22	0.5	8.8
				A657b_11	2.1	23	0.6	8.8
P18	1.8 ± 0.2 (8.7%)	92 ± 28 (30.0%)	2.1 ± 0.5 (24.6%)	A657b_07	1.6	60	1.7	6.7
				A657b_081	1.7	112	1.8	6.6
				A657b_09	2.0	64	2.9	7.5
				A657b_10	1.8	111	2.1	8.0
				A657b_11	1.8	114	1.7	8.0
P20	3.2 ± 0.5 (16.2%)	37 ± 50 (136.6%)	1.0 ± 1.7 (162.7%)	A658b_01	3.5	107	3.8	9.9
				A658b_02	2.7	74	1.3	9.8
				A658b_03	3.6	3	0.0	8.6
				A658b_041	2.5	0	0.0	6.4
				A658b_05	3.6	0	0.0	8.6
P21	7.0 ± 3.3 (47.6%)	160 ± 31 (19.4%)	1.3 ± 1.6 (121.1%)	A661b_06	3.3	138	4.0	10.5
				A661b_071	5.3	138	1.0	7.3
				A661b_08	5.3	138	1.0	7.3
				A661b_09	10.5	206	0.0	9.8
				A661b_10	10.5	176	0.5	9.9
P22	3.5 ± 0.5 (14.2%)	27 ± 3 (9.6%)	1.2 ± 0.2 (14.2%)	A662b_071	2.7	30	1.1	11.0
				A662b_08	3.6	25	1.1	15.3
				A662b_09	3.7	24	1.1	16.1
				A662b_10	3.9	27	1.4	18.7
				A662b_11	3.6	28	1.4	16.1

Shown in Figure 7 resp. 5.

samples (pit fill) (0.0029 resp. 0.0022), the lowest in the loess sample (0.0018) and increase again in the periglacial debris sample (0.0022). Thus, a clear pedogenic enrichment of iron is present in the topsoil and pit-fill and a dithionite soluble primary iron mineral in the lowest sample is probable to explain the increase of susceptibility within the deepest layer. The content of organic matter is the highest in the topsoil and in the pit fill (Figure 8(e)). Some carbonates are present in the loess, whereas the deepest sample contains very few organic matter and carbonates. The RGB colour values (Figure 8(f)) clearly reflect the darker colours of the pit fill and the organic surface horizon, whereas the lower two layers are more reddish brown. The sample from the pit fill (0.53–0.85 m) is the darkest layer.

The results of the laboratory analyses can be summarized as follows: The deepest sample (periglacial debris) has the highest susceptibility, however the frequency dependent susceptibility and the iron content by weight are the lowest. Moreover the contents of organic matter and carbonates are very low. The topsoil and pit filling have intermediate susceptibility values with a high frequency dependent susceptibility and a high content of organic matter and iron, whereas the content of carbonates is low. The loess has the lowest susceptibility value with an intermediate frequency dependent portion and an intermediate content of iron. As expected the content of organic matter is very low and the content of carbonates is the highest of all samples.

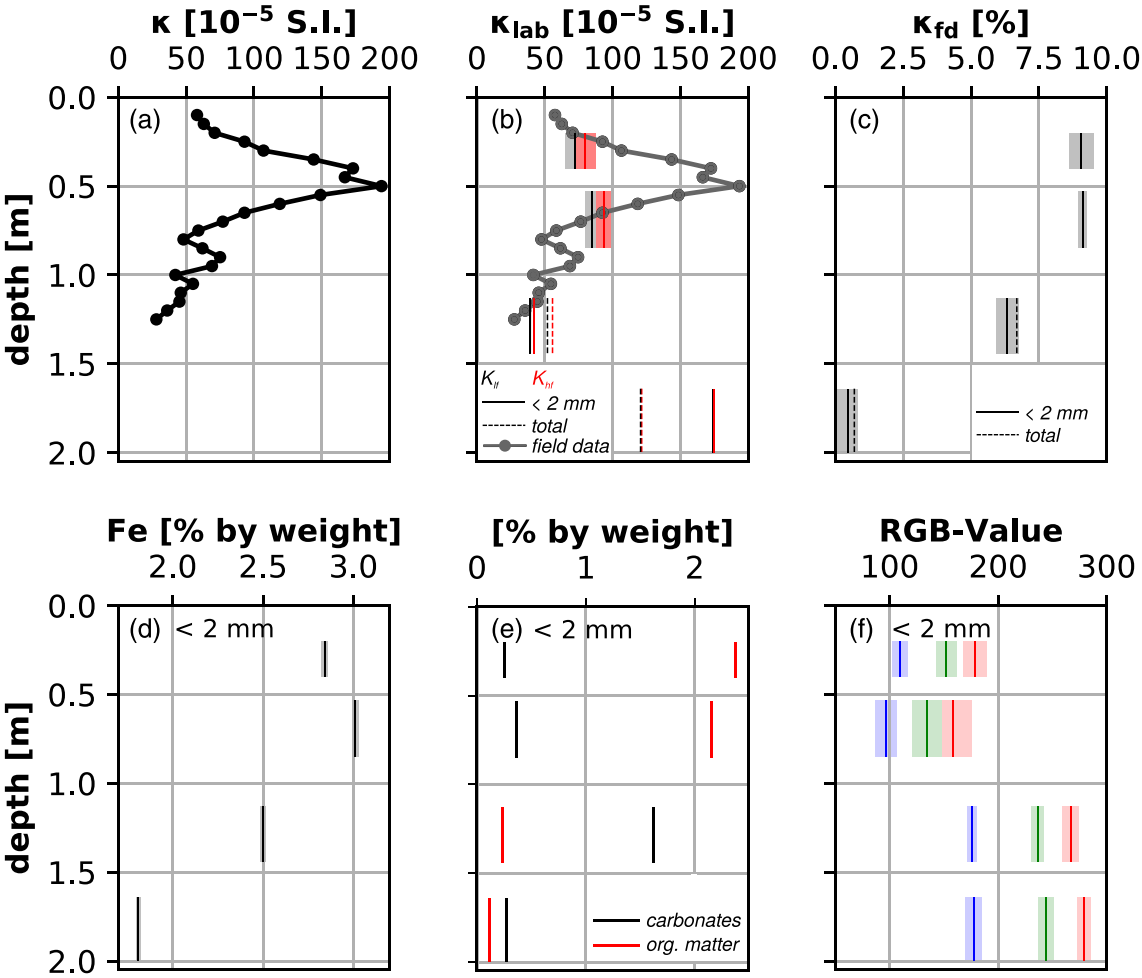

FIGURE 8 Data of coring P16_175 (location marked with a star in Figures 1 and 7). (a) Susceptibility downhole measurements. Laboratory measurements of (b) low frequency susceptibility and high frequency susceptibility for the fraction < 2 mm and the complete sample (with field measurements for comparison), (c) frequency dependent susceptibility, (d) iron content by weight resulting from XRF, (e) content of organic matter and carbonates, and (f) sample colour in red-green-blue (RGB) [scale 0–1023]. For the laboratory measurements the vertical line represents the mean value and the faded box the standard deviation for each mixed sample of the respective depth interval [Colour figure can be viewed at wileyonlinelibrary.com]

5 | DISCUSSION

In the discussion, we first address the methodical aspects of the inversion approach. Then we turn to the interpretation of the susceptibility distribution in combination with the derived Koenigsberger ratio to analyse the origin of remanence.

5.1 | Evaluation of the inversion approach and the results

We presented a novel inversion approach to determine the Koenigsberger ratio from magnetic field measurements (gradiometer data) and downhole measurements of the magnetic susceptibility, in which the susceptibility measurements constitute a variable basis function of the inversion. We have not found other studies, in which this sort of partial parameter coupling has been applied. Generally field studies of the Koenigsberger ratio are rare an exception being Benech et al. (2002).

For Q the cost function has a single, well-defined minimum and small trade-offs between different model parameters are observed. This shows that our approach yields reasonable values for the Koenigsberger ratio. The trade-off identified between t and l indicates that one of these model parameters should be determined by measurement. For example, the taper length l could be determined implicitly by extending the drilling profile far enough beyond the magnetic anomaly. In this case the complete subsurface section that contributes to the magnetic anomaly would be covered with downhole measurements and taper length l could even be omitted in the equations.

The percentage standard deviation per drilling profile (statistical evaluation B) is larger than the error of the single inversions (statistical

evaluation A). Therefore, the influence of different magnetic data sets yields a measure for the overall error.

For profile 16 higher trade-off values and generally higher RMS errors were observed. This probably indicates that the model was not complex enough to explain the observed magnetic anomalies. One possible reason is the approximation of actually three-dimensional susceptibility and remanence distributions with a two-dimensional susceptibility distribution and a parametrization of the remanence with three parameters. Another reason might be a significant contribution of the periglacial debris layer beneath the loess. The laboratory analyses showed that this layer has a high susceptibility. Moreover, the heterogeneity of a debris layer is likely reflected in a heterogeneous susceptibility distribution and possibly also a remanent magnetization. However, we were not able to measure the susceptibility distribution in this layer because it was not feasible to lower the probe. To investigate the magnetic properties of this layer, further studies can comprise test trenches or lined cores to gather undisturbed high-resolution samples for laboratory analyses.

For profile 21, especially high values for Q (4.2–11.2) were determined in combination with high values for t (149–186×10^{-5} SI). These locally very restricted areas of high susceptibility values might be related to burned material, i.e. daub or pottery. Both have been documented in the fillings of the pits. Our approach can be extended by an additional parameter for Q, that is only valid for remanent magnetization of heated materials.

5.2 | Remanent magnetization in archaeological prospecting

The starting point of our study was a simple check whether or not measured magnetic anomalies fit to calculated anomalies given the downhole-measured susceptibility distributions. This comparison is straightforward, yet not common in archaeological case studies. A similar approach was used by Bruce Bevan to quantify the magnetic anomaly of a potential structure (Dalan, 2008). The geometry of the feature approximated by a wedge and the initial susceptibility contrast for the inversion was derived from downhole susceptibility measurements, too. As in our case, the comparison of the measured and calculated magnetic anomaly showed that the susceptibility contrast was not sufficient to explain the observed anomaly. Instead, it needed to be increased from 45×10^{-5} SI to 140×10^{-5} SI. This also indicates a contribution from remanent magnetization (Dalan, 2008). Also Simon, Koziol, and Thiesson (2012) concluded that the measured susceptibility contrast for the modelled simplified source geometry is not high enough to explain the measured magnetic anomaly. With our approach, we offer a solution or an improvement to this mismatch problem in two regards: (1) a direct quantification of the Koenigsberger ratio and (2) the simplified source geometry with susceptibility contrasts is replaced by measured susceptibility distributions so that complex subsurface structures can be accessed.

As suggested by the equivalence principles of potential field theory, simplified magnetic source distributions (Miller et al., 2019; Wilken et al., 2015) are capable to explain observed anomalies in a satisfying way in many cases. However, our downhole measurements have shown that the assumption of a polygonal zone of constant susceptibility contrast would be an oversimplification of the filling of the neolithic pits. The measured susceptibility distributions are diverse and heterogeneous, hence too complex to be consistently approximated by a simple source geometry.

Generally, the Koenigsberger ratio and the remanent magnetization are not negligible (cf. Dalan, 2008; Simon et al., 2012). Still most modelling studies assume only induced magnetization. This is physically justified if the remanent magnetization is a pure VRM, which shows the same vector orientation as the induced magnetization. In this case neglecting remanent magnetization in inversion computations just leads to too high apparent or effective susceptibility values. Macnae (1994) discusses this issue from a mineral prospection perspective and proposes the use of an alternative ratio to Q. Anyway, for archaeological prospection purposes distinguishing between induced and remanent magnetization in field studies requires measurements of susceptibility preferably *in situ*. This can be accomplished by drilling or by additional EMI measurements if the EMI sounding depth is sufficiently large.

The drilling approach applied here can be optimized by investigating how dense the drilling locations need to be placed within the area of the considered anomaly. Also, a variable drilling spacing increasing from the edges to its surrounding can improve our approach. This can reduce the number of drillings needed to determine the susceptibility distribution. Placing an increased number of drillings outside the pits would also make the tapering parameter l obsolete as this part of the profile would get covered with downhole measurements.

5.3 | How do the derived Koenigsberger ratios compare to published values?

The Koenigsberger ratios of the best fitting models (Table 2) range from 1.6 to 10.5 with the majority of the values being smaller than 4. In archaeological studies the Koenigsberger ratio is usually determined for sites with burned contexts, such as kiln, ovens, fire places. Sometimes the studies include demagnetization in the measurement procedure to remove VRM. Schnepp et al. (2004) give an overview for archaeological sites in Germany. They divided the samples into three categories of structures heated to different temperatures (low, moderate and high). For all three categories the Koenigsberger ratio ranges from values of approximately 0.1 to values larger than 100. There seems to be a tentative tendency that for higher temperatures the majority of Q values shift to slightly higher values. The variability within the different categories, might indicate how well a specimen was heated. This means that high Koenigsberger ratios are measured for specimens carrying complete thermoremanent magnetization (Schnepp et al., 2004). However, also the parent material with its capability to carry remanent magnetization needs to be considered.

The Koenigsberger ratios determined in the present study can be understood as average values applying to larger volumes of

susceptible soil. The actual size and shape of each volume are determined by the threshold variable determined in the inversion. Therefore, this Koenigsberger ratio must be interpreted as value for a sample 'mixed' from larger soil volumes to be comparable with published measurements. In the present case, the subsurface does not show any traces of burning apart from sporadic daub pieces or pottery fragments. Therefore, the corresponding Koenigsberger ratios represent values of only partly or not heated soils and sediments with loess as parent material. We derived values that are within the range presented by Schnepp et al. (2004) with an approximate range of 0.1 to 10. Kapper, Donadini, et al. (2014) presented values closer to the here observed one from an archaeological context of burned cave sediments. However, in their study the majority of the values fall into the range of 0.1 to 1, which is considerably lower than the values found for the long pits of the Vráble site.

Without determining the Koenigsberger ratio, Batt (1999) measured the NRM of water-lain archaeological sediments of 30 depositional environments within Britain. For the NRM they obtained intensities in the range of burned materials. These results support the plausibility of the relatively high *Q*-values we obtained because the pit fills of our study can be considered as a similar depositional milieu.

5.4 | What is the origin of the remanence?

Several sources of remanent magnetization need to be considered, which may be distinguished into two groups according to the time frames of the generating processes. The first group consists of processes where the magnetized object and the bulk remanence form almost synchronously; these are here

- depositional remanence (e.g. Batt, 1999; Evans & Heller, 2003; Fassbinder, 2015),
- thermoremanent magnetization of daub pieces (e.g. Fassbinder, 2015), and
- organic matter decomposition processes in presence of magnetotactic bacteria (e.g. Blakemore, 1975; Fassbinder, Stanjekt, & Vali, 1990; Bazylinski, Lefèvre, & Schüler, 2013)

The second group consists of processes where the formation of bulk remanence extends over a much longer time span than the formation of the object as such, meaning by the on-going alignment of already existing magnetic moments, such as

- post-depostional remanence (e.g. Evans & Heller, 2003; Fassbinder, 2015; Batt, 1999) and
- viscous remanent magnetization (e.g. Dabas, Jolivet, & Tabbagh, 1992; Dunlop, 1973; Mullins & Tite, 1973; Néel, 1949; Néel, 1955)

Both, the observed depth functions of susceptibility and the deduced remanent magnetization within the organic infills of house-accompanying pits of the LBK houses at Vráble can be explained as a combination of these processes.

Depositional remanence results from the infilling of magnetized particles into the pit, which align in direction of the ambient magnetic field during the sedimentation process. Magnetized particles are produced in settlements, for example, in the form of ceramics and in the soil of fire places. The particles can get into the pit filling intentionally or unintentionally by waste disposal or aeolian transportation. If the particles are mobile within the pit filling, they can align in the direction of the earth's magnetic field and create a bulk remanent magnetization.

During the excavations, thin layers with a higher amount of daub were documented in the pits (cf. section 2.2). As they were not burned in place, the orientation of their initial remanent magnetization is unknown. However, the orientation might have turned partly parallel to the ambient field since the time of deposition due to viscous reorientation of the magnetic moments.

Magnetotactic bacteria were traditionally studied in freshwater (Blakemore, Maratea, & Wolfe, 1979; Spring et al., 1993) or marine environments (Petermann & Bleil, 1993; Stolz, Chang, & Kirschvink, 1986), but they have been detected in waterlogged soils as well (Fassbinder et al., 1990). There, magnetotactic bacteria were found to thrive close to or below the oxic–anoxic interface (Bazylinski et al., 2013). However, considering the habitat conditions of microorganisms in soils, a remarkable microscale variability of water and oxygen access has been documented (Hartmann & Simmeth, 1990; Hattori, 1973; Sexstone, Revsbech, Parkin, & Tiedje, 1985).

The infill of everyday waste, containing large amounts of organic matter, into the house-accompanying pits would have resulted in partial decomposition of the organic detritus under partly anoxic conditions. This is plausible considering the regional climate in eastern Slovakia, the form of the house-accompanying pits and the properties of their infill. The climate at Vráble is classified as cold-temperate (Köppen-Geiger Cfb) (Schönwiese, 1994) with an annual mean temperature of 9.9 °C and an annual sum of precipitation of 593 mm for the period 1982 to 2012 (http://www.climate%2010data.org, accessed 7 November 2019). Assuming similar conditions throughout the last 7000 years, results in an average excess of precipitation above evapotranspiration at the site. House-accompanying pits do not have an outlet nor are they sheltered from addition of water by precipitation (Dreibrodt et al., 2017), required for aerobic decomposition of organic matter according to technical instructions of pit composting (Misra, Roy, & Hiraoka, 2003). In fact, the orientation of the pits along the eaves of the LBK houses is even probable to increase the number and duration of waterlogging phases during the lifetime of the prehistoric house. In addition, after the abandonment of the houses, remainders of the pits completely filled or not, were enduring depressions of higher water content compared to the surrounding unbuilt areas. The infill of the pits, studied in numerous excavations, is mainly composed of a dark organic-mineral mixture, often resembling the local topsoil macroscopically (see Figure 2).

Thus, an organic rich infill as a growing medium for soil bacteria was provided by the prehistoric inhabitants and according to the

regional climatic conditions and configuration of the pits probably exposed to phases of anoxic decomposition. Additionally, anaerobic conditions could have been induced by high growing rates of aerobic soil bacteria populations on the organic rich infills consuming large amounts of oxygen. Micro-scale phenomena in infilled soil aggregates provide a third mechanism that could produce locally anaerobic conditions.

We argue that these phases of anaerobic decomposition of the organic trench-infills provided suitable living conditions for magnetotactic bacteria, which in turn resulted in the formation of ferrimagnetic iron compounds. Likewise to magnetic particles from settlement activities and thermoremanent compounds in daub, the remanent magnetization can orient parallel to the ambient field by rotation of mobile particles or the acquisition of a viscous remanent magnetization over time. The outlined scenario is able to explain our record. The typical site-specific downhole trend of susceptibility shows a minimum below the pit fills, increased values within the pit fill and a decrease towards the topsoil. This indicates that the process that resulted in the formation of the magnetic anomaly within the pit fill was not in action in the well-aerated topsoil, plowed additionally probably during approximately 2000 years since site formation (Dreibrodt et al., 2017). On the one hand, magnetotactic bacteria are known to be restricted to or close to anoxic environments (Bazylinski et al., 2013), on the other hand, the orientation of remanent magnetization is removed by the plowing or any bioturbation.

In summary, the remanent magnetization found by comparing observed magnetic anomalies and anomalies resulting from induced magnetization in this study is explainable by the outlined scenarios. Although we do not have direct proof, the contribution of magnetotactic bacteria in the decomposition process of the organic rich infill of the prehistoric pits provides a plausible explanation of the found remanent magnetization. The macroscopic reorientation of particles parallel to the earth's magnetic field and viscous remanent magnetization over time may provide further contributions, the relative portions of which still have to be investigated.

6 | CONCLUSIONS

Based on our study of the the Linearbandkeramik site Vráble 'Farské' the following conclusions can be derived:

1. Vertical sections of magnetic susceptibility determined from dense drillings and downhole measurements can be used to reliably image cross-sections of house-accompanying pits.
2. The remanent magnetizations of the pit fill and the surrounding loess are not negligible in the quantitative interpretation of magnetic surveys. The determined Koenigsberger ratios of the pit fills vary between 1.8 and 7.
3. Representative values of bulk remanent magnetization can be determined through a new inversion approach based on observed magnetic anomalies and *in situ* measurements of the susceptibility.
4. The origin of the remanent magnetization can be explained by magnetotactic bacteria and deposition of magnetized material. These particles increase the ferrimagnetic iron content of the pit fill compared to the surrounding, may align in the waterlogged environment and accumulate a viscous remanent magnetization.

Incorporating downhole susceptibility measurements in archaeological field campaigns enables an efficient ground truthing of magnetic mapping and determination of cross-sections of key targets. The same approach to determine bulk remanent magnetization can also be applied to archaeological plans as a tool of supporting excavation diagnostics.

ACKNOWLEDGEMENTS

We are grateful to the Deutsche Froschungsgemeinschaft (German Research Foundation - Project Number 2901391021 - Collaborative Research Centre 1266) for funding the presented research. The work discussed in this article was also funded by the Vedecká Grantová Agentúra MŠVVaŠ SR a SAV (VEGA-Project 2/0107/17) 'Civilization development and settlement structure during the Linear Pottery culture era in the lower Žitava basin'.

We gratefully acknowledge the help of Erica Corradini, Amelie Klein and especially Raphael Kahn while conducting all the manual drillings and measurements in the heat of summer 2018. Furthermore, we like to thank everybody who was involved in the field works that comprised any form of drilling and sampling as this data advected the image of the site although not presented here. We thank two anonymous reviewers for their constructive review and helpful suggestions.

ORCID

Natalie Pickartz https://orcid.org/0000-0002-3290-7032
Wolfgang Rabbel https://orcid.org/0000-0003-4720-6906
Knut Rassmann https://orcid.org/0000-0002-2570-6099
Nils Müller-Scheeßel https://orcid.org/0000-0001-7992-8722
Martin Furholt https://orcid.org/0000-0001-9998-6065
Tina Wunderlich https://orcid.org/0000-0003-2275-704X

REFERENCES

Allard, P., Hamon, C., Bonnardin, S., Cayol, N., Chartier, M., Coudart, A., … Thevenet, C. (2013). Linear Pottery domestic space: Taphonomy, distribution of finds and economy in the Aisne valley settlements. In C. Hamon, P. Allard, & M. Ilett (Eds.), *The domestic space in LBK settlements. Nanterre (France), 7–8 October 2010* (pp. 9–28). Rahden: M. Leidorf.

Batt, C. M. (1999). Preliminary investigations into the acquisition of remanence in archaeological sediments. *Geological Society, London, Special Publications, 151*, 9–19. https://doi.org/10.1144/GSL.SP.1999.151.01.02

Bazylinski, D. A., Lefèvre, C. T., & Schüler, D. (2013). Magnetotactic bacteria. *The Prokaryotes: Prokaryotic physiology and biochemistry* Berlin: Springer. 453–494.

Benech, C., Tabbagh, A., & Desvignes, G. (2002). Joint inversion of EM and magnetic data for near-surface studies. *Geophysics, 67*, 1729–1739. https://doi.org/10.1190/1.1527074

Blakemore, L., Searle, P., & Daly, B. (1987). Methods for chemical analysis of soils. In *Scientific report 80. New Zealand soil bureau*. New Zealand: Department of Scientific and Industrial Research.

Blakemore, R. (1975). Magnetotactic bacteria. *Science*, *190*, 377–379. https://doi.org/10.1126/science.170679

Blakemore, R., Maratea, D., & Wolfe, R. (1979). Isolation and pure culture of a freshwater magnetic spirillum in chemically defined medium. *Journal of Bacteriology*, *140*, 720–729. https://doi.org/10.1128/JB.140.2.720-729.1979

Branch, M. A., Coleman, T. F., & Li, Y. (1999). A subspace, interior and conjugate gradient method for large-scale bound-constrained minimization problems. *SIAM Journal on Scientific Computing*, *21*, 1–23. https://doi.org/10.1137/S1064827595289108

Carrancho, Á., Villalaín, J. J., Angelucci, D., Dekkers, M. J., Vallverdú, J., & Vergès, J. M. (2009). Rock-magnetic analyses as a tool to investigate archaeological fired sediments: A case study of mirador cave (Sierra de Atapuerca, Spain). *Geophysical Journal International*, *179*, 79–96. https://doi.org/10.1111/j.1365-246X.2009.04276.x

Catanzariti, G., McIntosh, G., Soares, A. M. M., Díaz-Martínez, E., Kresten, P., & Osetea, M. L. (2008). Archaeomagnetic dating of a vitrified wall at the Late Bronze Age settlement of Misericordia (Serpa, Portugal). *Journal of Archaeological Science*, *35*, 1399–1407. https://doi.org/10.1016/j.jas.2007.10.004

Dabas, M., Jolivet, A., & Tabbagh, A. (1992). Magnetic susceptibility and viscosity of soils in a weak time varying field. *Geophysical Journal International*, *108*, 101–109. https://doi.org/10.1111/j.1365-246X.1992.tb00841.x

Dalan, R. A. (2008). A review of the role of magnetic susceptibility in archaeogeophysical studies in the USA: Recent developments and prospects. *Archaeological Prospection*, *15*, 1–31. https://doi.org/10.1002/arp.323

Dean, W. E. (1974). Determination of carbonate and organic matter in calcareous sediments and sedimentary rocks by loss on ignition; comparison with other methods. *Journal of Sedimentary Research*, *44*, 242–248.

Dreibrodt, S., Furholt, M., Hofmann, R., Hinz, M., & Cheben, I. (2017). P-Ed-XRF-geochemical signatures of a 7300 year old linear band pottery house ditch fill at Vráble-Ve'lké Lehemby, Slovakia – house inhabitation and post-depositional processes. *Quaternary International*, *438*, 131–143. https://doi.org/10.1016/j.quaint.2017.03.054

Dunlop, D. J. (1973). Theory of the magnetic viscosity of lunar and terrestrial rocks. *Reviews of Geophysics*, *11*, 855–901. . https://doi.org/10.1029/RG011i004p00855

Eckelmann, W., Sponagel, H., Grottenthaler, W., Hartmann, K. J., Hartwich, R., Janetzko, P., … Traidl, R. (2006). *Bodenkundliche Kartieranleitung KA5*. Stuttgart: Schweizerbart Science Publishers.

Ertepinar, P., Langereis, C. G., Biggin, A. J., de Groot, L. V., Kulakoglu, F., Omura, S., & Süel, A. (2016). Full vector archaeomagnetic records from Anatolia between 2400 and 1350 BCE: Implications for geomagnetic field models and the dating of fires in antiquity. *Earth and Planetary Science Letters*, *434*, 171–186. https://doi.org/10.1016/j.epsl.2015.11.015

Evans, M. E., & Heller, F. (2003). *Environmental magnetism: Principles and applications of enviromagnetics*. International Geophysics SeriesAmsterdam: . Academic Press.

Fassbinder, J. W. (2015). Seeing beneath the farmland, steppe and desert soil: magnetic prospecting and soil magnetism. *Journal of Archaeological Science*, *56*, 85–95. https://doi.org/10.1016/j.jas.2015.02.023

Fassbinder, J. W. E., Stanjekt, H., & Vali, H. (1990). Occurrence of magnetic bacteria in soil. *Nature*, *343*, 161–163. https://doi.org/10.1038/343161a0

Furholt, M., Bátora, J., Cheben, I., Kroll, H., Rassmann, K., & Tóth, P. (2014). Vráble-Velké Lehemby: Eine Siedlungsgruppe der Linearkeramik in der Südwestslowakei. Vorbericht über die Untersuchungen der Jahre 2010 und 2012 und Deutungsansätze. *Slovenská Archeológia*, *62*, 227–266.

Gómez-Paccard, M., Catanzariti, G., Ruiz-Martínez, V. C., McIntosh, G., Núñez, J. I., Osete, M. L., … Thiriot, J. (2006). A catalogue of Spanish archaeomagnetic data. *Geophysical Journal International*, *166*, 1125–1143. https://doi.org/10.1111/j.1365-246X.2006.03020.x

Hartmann, A., & Simmeth, I. (1990). Einfluss des Bodenwasserpotentials auf die Lokalisation mikrobieller Aktivität in Bodenaggregaten eines ariden Sandlößbodens. *Mitteilungen der Deutschen Bodenkundlichen Gesellschaft*, *62*, 39–42.

Hattori, T. (1973). Microbial life in the soil: An introduction. *Technical report*.

Herries, A., Kovacheva, M., & Kostadinova, M. (2008). Mineral magnetism and archaeomagnetic dating of a mediaeval oven from Zlatna Livada, Bulgaria. *Physics and Chemistry of the Earth, Parts A/B/C*, *33*, 496–510. https://doi.org/10.1016/j.pce.2008.02.021

Hunt, C. P., Moskowitz, B. M., & Banerjee, S. K. (2013). *Magnetic properties of rocks and minerals* (pp. 189–204). Washington, D.C.: American Geophysical Union.

Jordanova, N., Kovacheva, M., & Kostadinova, M. (2004). Archaeomagnetic investigation and dating of Neolithic archaeological site (Kovachevo) from Bulgaria. *Physics of the Earth and Planetary Interiors*, *147*, 89–102.

Jrad, A., Quesnel, Y., Rochette, P., Jallouli, C., Khatib, S., Boukbida, H., & Demory, F. (2014). Magnetic investigations of buried palaeohearths inside a palaeolithic cave (Lazaret, Nice, France): Magnetic study of Lazaret palaeohearths. *Archaeological Prospection*, *21*, 87–101. https://doi.org/10.1002/arp.1469

Kainz, J., & Cotter, J. P. (2018). A broad band magnetic susceptibility test study — the magnetic spectroscopy of a neolithic ditch. *Journal of Archaeological Science: Reports*, *18*, 139–150. https://doi.org/10.1016/j.jasrep.2018.01.006

Kapper, K. L., Anesin, D., Donadini, F., Angelucci, D. E., Cavulli, F., Pedrotti, A., & Hirt, A. M. (2014). Linking site formation processes to magnetic properties. Rock- and archeomagnetic analysis of the combustion levels at Riparo Gaban (Italy). *Journal of Archaeological Science*, *41*, 836–855. https://doi.org/10.1016/j.jas.2013.10.015

Kapper, K. L., Donadini, F., Mauvilly, M., Panovska, S., & Hirt, A. M. (2014). New directional archeomagnetic data of burned cave sediments from Switzerland and geomagnetic field variations in central Europe. *Geophysical Journal International*, *198*, 1208–1221. https://doi.org/10.1093/gji/ggu184

Koenigsberger, J. G. (1930). Größenverhältnis von remanentem zu induziertem Magnetismus in Gesteinen; Größe und Richtung des remanenten Magnetismus. *Zeitschrift für Geophysik*, *6*, 190–207.

Koenigsberger, J. G. (1934). Magnetische Eigenschaften der ferromagnetischen Mineralien in den Gesteinen. *Beiträge Zur Angewandten Geophysik*, *4*, 385–394.

Koenigsberger, J. G. (1936). Die Abhängigkeit der natürlichen remanenten Magnetisierung bei Eruptivgesteinen von deren Alter und Zusammensetzung. *Beiträge Zur Angewandten Geophysik*, *5*, 193–246.

Kvetina, P., & Rídký, J. (2017). Neolithic settlement space waste, deposition and identity. In D. Sosna & L. Brunclíková (Eds.), *Archaeologies of waste: Encounters with the unwanted* (pp. 127–144). Oxford: Oxbow Books.

Linford, N. T., & Canti, M. G. (2001). Geophysical evidence for fires in antiquity: preliminary results from an experimental study. Paper given at the EGS XXIV General Assembly in The Hague, April 1999. *Archaeological Prospection*, *8*, 211–225. https://doi.org/10.1002/arp.170

Macnae, J. (1994). Viscous magnetization: Misleading Koeningsberger's Q. In *SEG technical program expanded abstracts 1994* (pp. 456–458). Society of Exploration Geophysicists.

Martińez, M., Lana, X., Olarte, J., Badal, J., & Canas, J. (2000). Inversion of Rayleigh wave phase and group velocities by simulated annealing. *Physics of the Earth and Planetary Interiors*, *122*, 3–17. https://doi.org/10.1016/S0031-9201(00)00183-7

Meadows, J., Müller-Scheeßel, N., Cheben, I., Rose, H., & Furholt, M. (2019). Temporal dynamics of Linearbandkeramik houses and

settlements, and their implications for detecting the environmental impact of early farming. *The Holocene*, *29*, 1653–1670. https://doi.org/10.1177/0959683619857239

Miller, B. K., Miller, B. K., Furholt, M., Bayarsaikhan, J., Tüvshinjargal, T., Brandtstätter, L., … Wunderlich, T. (2019). Proto-urban establishments in inner Asia: Surveys of an Iron Age walled site in eastern Mongolia. *Journal of Field Archaeology*, *44*, 267–286. https://doi.org/10.1080/00934690.2019.1598170

Misra, R., Roy, R., & Hiraoka, H. (2003). On-farm composting methods. *Technical report*, Rome: UN-FAO.

Müller-Scheeßel, N., Cheben, I., Filipovic, D., Hukelová, Z., &Furholt, M. (in press). The LBK site of Vráble in southwestern Slovakia: Selected results of the excavation season 2016. Ber. RGK, 97.

Müller-Scheeßel, N., Müller, J., Cheben, I., Mainusch, W., Rassmann, K., Rabbel, W., … Furholt, M. (2020). A new approach to the temporal significance of house orientations in european early neolithic settlements. *PLoS ONE*, *15*, e0226082. https://doi.org/10.1371/journal.pone.0226082

Mullins, C. E., & Tite, M. S. (1973). Magnetic viscosity, quadrature susceptibility, and frequency dependence of susceptibility in single-domain assemblies of magnetite and maghemite. *Journal of Geophysical Research*, *78*, 804–809.

Néel, L. (1949). Théorie du traînage magnétique des ferromagnétiques en grains fins avec applications aux terres cuites. *Annals De Geophysique*, *5*, 99–136.

Néel, L. (1955). Some theoretical aspects of rock-magnetism. *Advances in Physics*, *4*, 191–243. https://doi.org/10.1080/00018735500101204

Pavón-Carrasco, F. J., Osete, M. L., & Torta, J. M. (2010). Regional modeling of the geomagnetic field in Europe from 6000 to 1000 B.C. *Geochemistry, Geophysics, Geosystems*, *11*. https://doi.org/10.1029/2010GC003197

Petermann, H., & Bleil, U. (1993). Detection of live magnetotactic bacteria in South Atlantic deep-sea sediments. *Earth and Planetary Science Letters*, *117*, 223–228. https://doi.org/10.1016/0012-821X(93)90128-V

Pickartz, N., Corradini, E., Kahn, R., Panning, D., Rassmann, K., Müller-Scheeßel, N., & Rabbel, W. (2020). Extending archaeological documentation from 2D to 3D: The benefits of geophysical on-site measurements in excavations. In M. Furholt, I. Cheben, J. Müller, A. Bistáková, M. Wunderlich, & N. Müller-Scheeßel (Eds.), *Archaeology in the Žitava valley I – the LBK and Želiezovce settlement site of Vráble*. Leiden: Sidestone Press.

Plouff, D. (1976). Gravity and magnetic fields of polygonal prisms and application to magnetic terrain corrections. *Geophysics*, *41*, 727–741. https://doi.org/10.1190/1.1440645

Rabenhorst, M., Schmehling, A., Thompson, J. A., Hirmas, D. R., Graham, R. C., & Rossi, A. M. (2014). Reliability of soil color standards. *Soil Science Society of America Journal*, *79*, 193–199.

Sanmartín, P., Chorro, E., Vázquez-Nion, D., Martínez-Verdú, F. M., & Prieto, B. (2014). Conversion of a digital camera into a non-contact colorimeter for use in stone cultural heritage: The application case to Spanish granites. *Measurement*, *56*, 194–202. https://doi.org/10.1016/j.measurement.2014.06.023

Schneider, M., Linzen, S., Schiffler, M., Pohl, E., Ahrens, B., Dunkel, S., … Baumgarten, D. (2014). Inversion of geo-magnetic SQUID gradiometer prospection data using polyhedral model interpretation of elongated anomalies. *IEEE Transactions on Magnetics*, *50*, 1–4. https://doi.org/10.1109/TMAG.2014.2320361

Schnepp, E., & Pucher, R. (1998). Preliminary archaeomagnetic results from a floor sequence of a bread kiln in Lübeck (Germany). *Studia Geophysica et Geodaetica*, *42*, 1–11. https://doi.org/10.1023/A:1023348920652

Schnepp, E., Pucher, R., Reinders, J., Hambach, U., Soffel, H., & Hedley, I. (2004). A German catalogue of archaeomagnetic data. *Geophysical Journal International*, *157*, 64–78. https://doi.org/10.1111/j.1365-246X.2004.02163.x

Schönwiese, C.-D. (1994). *Klimatologie*. Stuttgart: Ulmer Verlag.

Sexstone, A. J., Revsbech, N. P., Parkin, T. B., & Tiedje, J. M. (1985). Direct measurement of oxygen profiles and denitrification rates in soil aggregates 1. *Soil Science Society of America Journal*, *49*, 645–651. https://doi.org/10.2136/sssaj1985.03615995004900030024x

Simon, F.-X., Koziol, A., & Thiesson, J. (2012). Investigating magnetic ghosts on an early middle age settlement: Comparison of data from stripped and non-stripped areas: Magnetic ghosts on an early middle age settlement. *Archaeological Prospection*, *19*, 191–200. https://doi.org/10.1002/arp.1427

Spring, S., Amann, R., Ludwig, W., Schleifer, K.-H., van Gemerden, H., & Petersen, N. (1993). Dominating role of an unusual magnetotactic bacterium in the microaerobic zone of a freshwater sediment. *Applied and Environmental Microbiology*, *59*, 2397–2403. https://doi.org/10.1128/AEM.59.8.2397-2403.1993

Stolz, J. F., Chang, S.-B. R., & Kirschvink, J. L. (1986). Magnetotactic bacteria and single-domain magnetite in hemipelagic sediments. *Nature*, *321*, 849–851. https://doi.org/10.1038/321849a0

Thébault, E., Finlay, C., Beggan, C., Alken, P., Aubert, J., Barrois, O., … Zvereva, T. (2015). International geomagnetic reference field: The 12th generation. *Earth, Planets and Space*, *67*, 67–79.

Uieda, L., Oliveira Jr, V. C., & Barbosa, V. C. (2013). Modeling the earth with fatiando a terra. In *Proceedings of the 12th Python in Science Conference* (eds. S. van der Walt, J. Millman and K. Huff), 96–103.

Wilken, D., & Rabbel, W. (2012). On the application of particle swarm optimization strategies on scholte-wave inversion: Pso in scholte-wave inversion. *Geophysical Journal International*, *190*, 580–594. https://doi.org/10.1111/j.1365-246X.2012.05500.x

Wilken, D., Wunderlich, T., Majchczack, B., Andersen, J., & Rabbel, W. (2015). Rayleigh-wave resonance analysis: a methodological test on a viking age pit house: Seismic resonance analysis on a pit house. *Archaeological Prospection*, *22*, 187–206. https://doi.org/10.1002/arp.1508

Wolfram, S. (2013). Two sides of the coin: ceramic taphonomy and domestic space in the Linear Pottery settlements Hanau-Klein-Auheim and Eythra (Germany). In C. Hamon, P. Allard, & M. Ilett (Eds.), *The domestic space in LBK settlements. Nanterre (France), 7–8 October 2010* (pp. 79–90). Rahden: M. Leidorf.

How to cite this article: Pickartz N, Rabbel W, Rassmann K, et al. What over 100 drillings tell us: a new method for determining the Koenigsberger ratio of soils from magnetic mapping and susceptibility logging. *Archaeological Prospection*. 2020;1–22. https://doi.org/10.1002/arp.1782

APPENDIX A: EVALUATION OF INVERSION RESULTS

To quantify the reliability of the models, we use two statistical approaches. With the first one (A), we test if the single inversion problem (one magnetic profile) is multimodal and if trade-offs between different model parameters exist. For this we use the Gibbs' distribution to calculate so-called expected model parameters, standard deviations and co-variances. With the second one (B), we test the influence of different magnetic profiles that are close to the drilling profile. The arithmetic mean and the standard deviation of the inversion parameters for each drilling profile are the final results.

A.1 | Methods

A.1.1 | Statistical evaluation (A) – Gibbs' distribution

Following the descriptions by for example Martińez, Lana, Olarte, Badal, and Canas, (2000) and Wilken and Rabbel (2012), a set of expected model parameters can be calculated considering the Gibbs' distribution as probability density function. To test whether the inversion result is influenced by the starting parameters, we defined a bounded model parameter space and passed through this space systematically with the sets of starting parameters. Hereby, each of the three model parameters had five equidistantly spaced starting values. This results in 125 combinations and inversion runs for each magnetic profile. For the statistical evaluation of the inversion problem, we considered not only the final inversion results but also every set of parameters being an intermediate step of the inversion process. This results in a total number of R models for each inversion. Let m_k be a set of model parameters (Q_k, t_k, l_k) with k = 1,...,R with the respective cost $L_k = L(m_k)$. Then,

$$\xi(m_k) = \exp[-L_k] \tag{A1}$$

is the probability of m_k. The expected model is then

$$< m > = \frac{1}{P}\sum_{k=1}^{R} m_k \xi(m_k) \tag{A2}$$

with the normalization factor

$$P = \sum_{k=1}^{R} \exp[-L_k]. \tag{A3}$$

The covariance matrix is

$$C_m = \frac{1}{P}\sum_{k=1}^{R} (m_k - < m >)(m_k - < m >)^T \xi(m_k) \tag{A4}$$

where the entries on the diagonal are the variances of each parameter. Hence, the standard deviation of the expected model parameters $<m>_i$ is $\sigma_i = \sqrt{C_{i,i}}$. To evaluate the correlation or possible trade-off between two parameters, the normalized covariance matrix

$$C_{i,j} = \frac{C_{i,j}}{\sqrt{C_{i,i} \cdot C_{j,j}}} \tag{A5}$$

is considered.

A.1.2 | Statistical evaluation (B) – arithmetic mean

The drilled profiles are approximately parallel to the magnetic profiles of the single sensors of the magnetic sensor array and orthogonal to

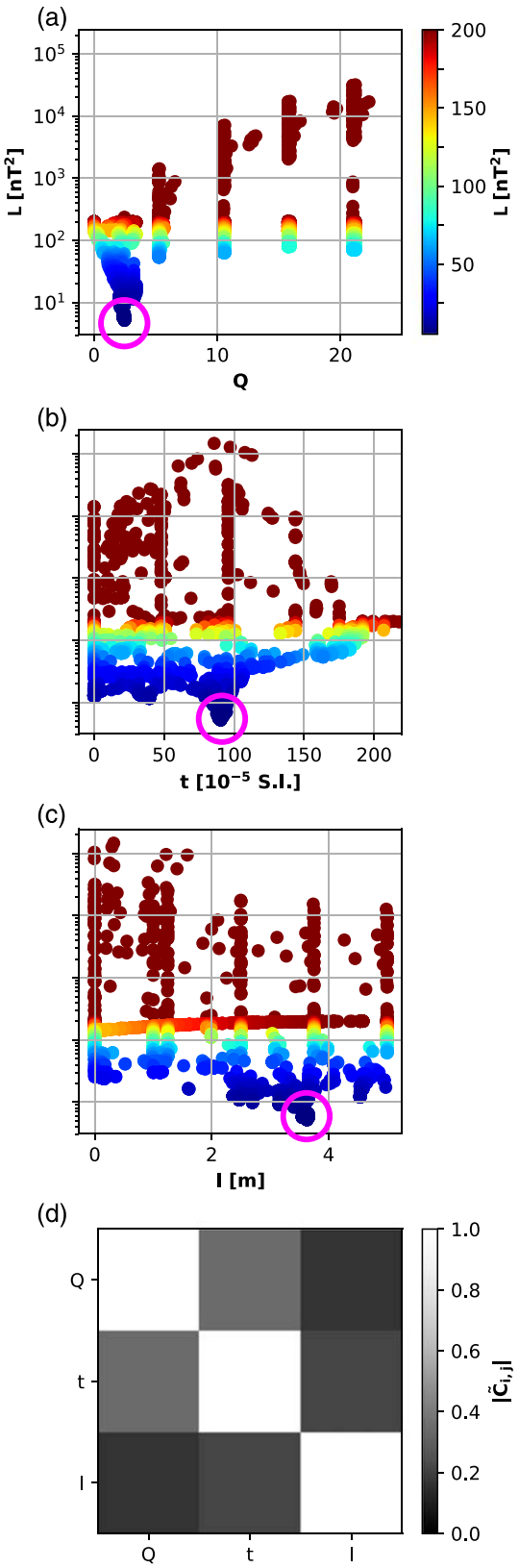

FIGURE 9 Model parameters (a) Koenigsberger ratio Q, (b) threshold t and (c) taper length l *versus* cost L for drilling profile P04 and magnetic profile A802b_03. (d) Correlation matrix for this profile [Colour figure can be viewed at wileyonlinelibrary.com]

the house-accompanying pits, which can be regarded as quasi two-dimensional structure. Therefore, we repeated the inversion computation for the five single sensor profile lines closest to the drilling profile (Figure 4A). The RMS error

$$\delta B_{RMS} = \sqrt{\frac{\sum_{i=1}^{N}\left(\Delta B_z^{obs,i} - \Delta B_z^{syn,i}\right)^2}{N}}, \tag{A6}$$

is used to identify the best fitting model for each of the five magnetic profiles. This results in five best fitting models for each drilling profile and enables an estimation of an arithmetic mean with standard deviation for each inversion parameter and drilling profile.

A.2 | Results – profile P04

The statistical evaluation (A) for drilling profile P04 and the magnetic profile A802b_03 yields the expected model parameters Q = 2.4 ± 0.1 (2.8%), t = 90 ± 3 × 10^{-5}SI (3.8%) and l = 3.6 ± 0.1m (2.8%). Figure 9(a–c) shows the intermediate steps and converged models with the respective cost for all model parameters. The cost function is unimodal for all model parameters, which means it shows one well-defined minimum in the model parameter space (cf. circles in Figure 9). Also there is no significant trade-off between the model parameters with trade-off values < 0.4 as visible in the covariance matrix in Figure 9(d).

To evaluate how well the model parameters are resolved, we consider a fit within twice the sensor resolution (±2 × 0.2 nT) as equally well fitted. Then the synthetic data is $\Delta B_z^{syn,i} = \Delta B_z^{obs,i} + 2cdot0.2$nT and for the cost follows $L_{res} = N(2 \times 0.2nT)^2$ where N is the number of observation points. Figure 10 shows the model parameters *versus* each other and the respective cost values. All models shown in green are equally well fit to the observed data. For Q the variability is small and therefore Q is well resolved. Contrasting to this, l and t show a higher variability. This is also reflected by the higher trade-off between t and l (cf. Figure 9(d)).

The optimum fitting parameters by RMS (statistical evaluation B) of drilling profile P04 with magnetic profile A802b_03 (Figure 5) is a Koenigsberger ratio of Q = 2.4, applied to soil volumes with a susceptibility of $\kappa \geq 90 \times 10^{-5}$ SI and a lateral taper with length l = 3.7 m. These are identical to the expected model parameters within their standard deviation. The resulting magnetic anomaly of induced and remanent magnetization has a maximum of approximately 7.0 nT (observed 7.2 nT) and the RMS error is reduced to 0.4 nT. The arithmetic means of the model parameters over the best fitting models for the different magnetic profiles for the drilling profile P04 are Q = 2.3 ± 0.3 (14.8%), t = 100 ± 6 × 10^{-5}SI (6.3%) and l = 3.9 ± 0.9m (22.8%). These errors are larger than those of the expected values for the inversions of a single magnetic profile. Therefore, the overall error is determined by the deviation resulting from different magnetic datasets.

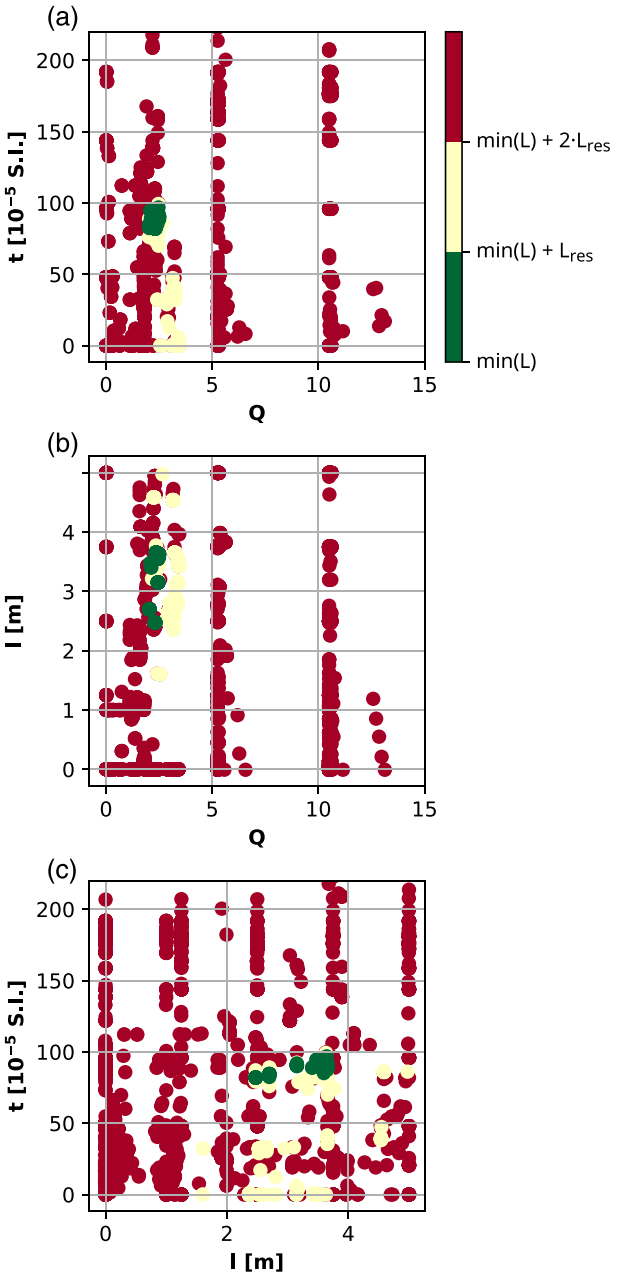

FIGURE 10 Comparison of model parameters *versus* each other for drilling profile P04 and magnetic profile A802b_03. The cost indicates the fit of the respective model response to the observed data with values in green in the interval between the lowest cost and the lowest cost plus L_{res}. (a) Koenigsberger ratio Q *versus* threshold t, (b) Q *versus* taper length l, (c) l *versus* t [Colour figure can be viewed at wileyonlinelibrary.com]

APPENDIX B: SYNTHETIC CASE STUDY

With this synthetic case study, we aim to evaluate the importance of the direction of the remanent magnetization. For this we define a schematic house-accompanying pit as a cuboid with a width of 3.0 m and a length of 18.0 m. It is buried 0.6 m under the surface and 0.6 m

thick. It is rotated 18° clockwise, which is approximately the rotation of the real features. For the pit, we assume a susceptibility that is 200 $\times 10^{-5}$ SI higher than the background. In addition, the pit has a remanent magnetization with a Koenigsberger ratio $Q = 3$.

We compare the synthetic anomalies for two cases: (1) the remanence is oriented in the same direction as the recent earth's magnetic field and (2) the remanence is oriented so that the largest possible difference to the recent orientation results. The variation of the D, I and B with an error band at 95% of the confidence level during the settlement period of the site is shown in Figure 11 derived from the SCHA.DIF.8 K model (Pavón-Carrasco et al., 2010). For the largest difference between recent and ancient magnetic field parameters, we used $D = 55.56°$ and $I = 4.21°$ dating to 5120 BCE. For the synthetic study the variation of the magnetic field strength is neglected since this can equally be represented by a variation of Q. Therefore, a change in B is not distinguishable from a change in Q. The forward calculations are conducted with the formula by Plouff (1976) as implemented in the Python-library 'Fatiando a Terra' (Uieda et al., 2013).

Figure 12 shows the synthetic anomaly of the model with the remanence oriented in recent (Figure 12(a)) and past (Figure 12(b)) orientation of the earth's magnetic field. The difference is depicted in Figure 12(c) and has a maximum of 1.6 nT. According to the manufacturer, the magnetic sensors have a resolution of 0.2 nT. However, taking field conditions with a motorized system into account, it is doubtful that the difference arising from a different orientation of the remanent compared to the induced magnetization is detectable

In conclusion this modelling study shows, that the approximation of the orientation of the remanence in direction of the recent earth's magnetic field is permissible.

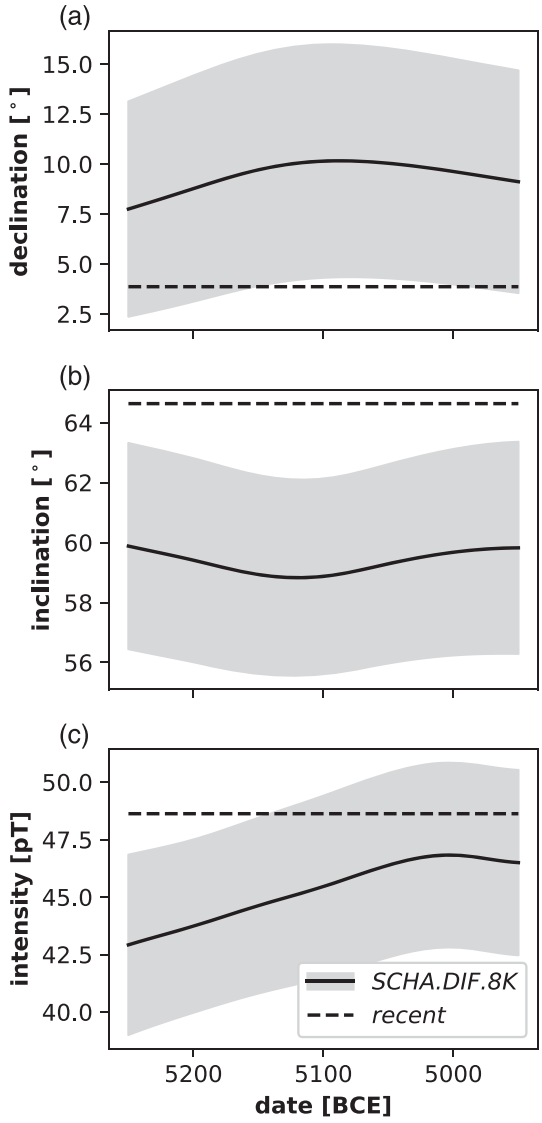

FIGURE 11 Declination (a), inclination (b) and intensity (c) of the earth's magnetic field during the inhabited time of the settlement (Pavón-Carrasco et al., 2010) in comparison to the recent parameters (Thébault et al., 2015)

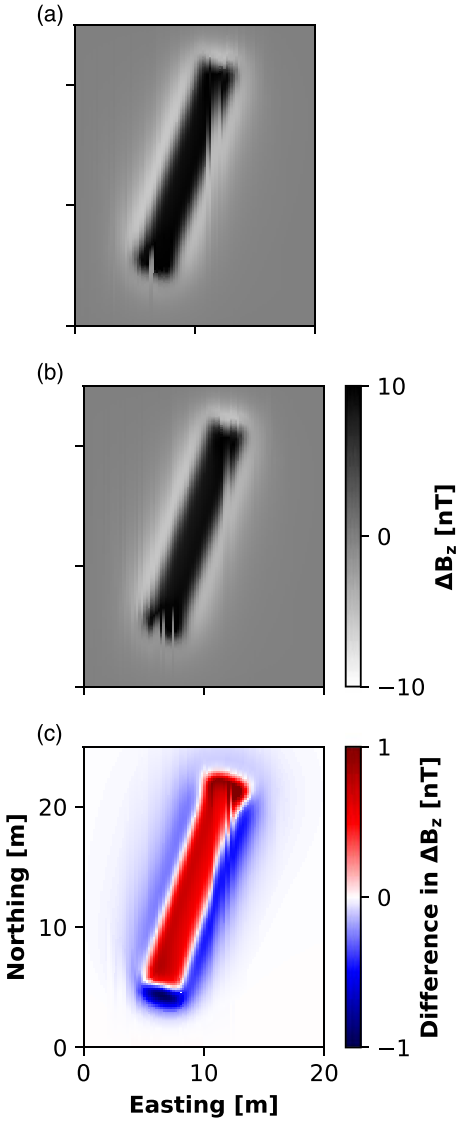

FIGURE 12 Synthetic anomaly of a schematic pit model for (a) recent orientation and (b) past orientation of the remanent magnetization. (c) Difference between these two cases [Colour figure can be viewed at wileyonlinelibrary.com]